DTID FILE COPY

AD-A222 435

TION PAGE

Form Approved
OMB No. 0704-0188

erage 1 hour per response, including the time for reviewing instructions, searching existing data sources,
the collection of information. Send comments regarding this burden estimate or any other aspect of this
s Washington Headquarters Services, Directorate for Information Operations and Reports, 1215 Jefferson
Management and Budget, Paperwork Reduction Project (0704-0188), Washington, DC 20503.

1. AGENCY USE ONLY (Leave blank)	2. REPORT DATE 21 May 1990	3. REPORT TYPE AND DATES COVERED Final Report/1 Mar 87-28 Feb 90

4. TITLE AND SUBTITLE The Near-Earth Orbital Environment Coupling to its Energy Sources	5. FUNDING NUMBERS 61102F/2311/A1

6. AUTHOR(S) William Olsen	

7. PERFORMING ORGANIZATION NAME(S) AND ADDRESS(ES) McDonnell Douglas Corp 5301 Bolsa Avenue Huntington Beach CA 92647	8. PERFORMING ORGANIZATION REPORT NUMBER AEOSR-TR· 90 0658

9. SPONSORING/MONITORING AGENCY NAME(S) AND ADDRESS(ES) AFOSR/NP Bolling AFB DC 20332-6448	10. SPONSORING/MONITORING AGENCY REPORT NUMBER F49620-87-C-0039

11. SUPPLEMENTARY NOTES

12a. DISTRIBUTION/AVAILABILITY STATEMENT Approved for public release; distribution is unlimited.	12b. DISTRIBUTION CODE

13. ABSTRACT (Maximum 200 words)

Under the present study the qualitative work performed earlier has been extended to perform quantitative calculations of the entry of plasma into the magnetosphere. These calculations include the structure of the low-latitude boundary layer and the energy spectrum of the particles within the plasma sheet. These calculations were performed using actual satellite data and virtually no assumed parameters. The success of these calculations provides impressive evidence for the validity of the Gradient Drift Entry theory. It also proves that the widely held notion that the magnetosheath cannot be the source of plasma sheet particles is in error. The success of this studey permits the development of quantitative models of the magnetosphere required for the prediction of magnetospheric and upper atmospheric and ionospheric effects on those hardware systems which must operate in Earth orbital space.

14. SUBJECT TERMS Magnetosphere, Substorm, Gradient Drift	15. NUMBER OF PAGES 75
	16. PRICE CODE

17. SECURITY CLASSIFICATION OF REPORT UNCLASSIFIED	18. SECURITY CLASSIFICATION OF THIS PAGE UNCLASSIFIED	19. SECURITY CLASSIFICATION OF ABSTRACT UNCLASSIFIED	20. LIMITATION OF ABSTRACT UL SAR

NSN 7540-01-280-5500

Standard Form 298 (Rev. 2-89)
Prescribed by ANSI Std. Z39-18

The Near-Earth Orbital Environment Coupling to its Energy Sources

MCDONNELL
DOUGLAS
CORPORATION

Final Report
(0002AA)

AEOSR-TR· 90 0658

April 1990

F49620-87-C-0039

Co-Investigators:

S. L. Huston
K. A. Pfitzer
T. S. Mogstad

Principal Investigator:

W. P. Olson, Director
Design & Technology Center

MCDONNELL DOUGLAS SPACE SYSTEMS COMPANY
DESIGN & TECHNOLOGY CENTER
5301 Bolsa Avenue Huntington Beach, California 92647 (714) 896-3311

90 06 04 129

FOREWORD

This final report describes progress in our work on the interactions between the interplanetary region (notably the solar wind) and the Earth's magnetosphere.

In previous papers and reports we have described the Gradient Drift Entry theory of the formation and maintenance of the "ground state" of the magnetosphere. We have explained qualitatively how the magnetosphere is maintained by the entry of solar wind plasma along the flanks of the magnetotail and in the dayside cusp regions. Clearly, this single particle theory can explain many magnetospheric features if it can be quantitatively formulated for large numbers of particles. The work of Craig Olson on the penetration of charged particle beams into magnetic field regions has been used to develop a quantitative formalism that physically ties the magnetosphere to its magnetosheath (shocked solar wind) particle source.

Under the present study we have extended the qualitative work performed earlier to perform quantitative calculations of the entry of plasma into the magnetosphere. These calculations include the structure of the low-latitude boundary layer and the energy spectrum of the particles within the plasma sheet. These calculations were performed using actual satellite data and virtually no assumed parameters. The success of these calculations provides impressive evidence for the validity of the GDE theory. It also proves that the widely held notion that the magnetosheath cannot be the source of plasma sheet particles is in error.

The success of this study places us in the position to develop quantitative models of the magnetosphere required for the prediction of magnetospheric and upper atmospheric and ionospheric effects on those hardware systems which must operate in Earth orbital space.

A version of this final report has been submitted for publication in *Journal of Geophysical Research*.

Contents

Section 1

BACKGROUND AND INTRODUCTION

In our previous progress reports, we demonstrated that solar wind plasma can enter the magnetosphere through the gradient drift entry (GDE) process and investigated some of the features of the resulting plasma flow within the magnetosphere. These calculations included models of the low-latitude boundary layer (LLBL) and the LLBL electric field; these models used LLBL thickness and electric field which were representative of observed values. In reality, the LLBL thickness and potential arc determined by the GDE process, but these earlier calculations were not self-consistent.

During the present study, self-consistent calculations of plasma entry were performed; a "map" of particle entry in the tail was developed; and procedures were developed which self-consistently determined the flux of particles entering the magnetosphere, the LLBL thickness and potential, and the magnitude of the the Birkeland and plasma sheet currents. The properties of the LLBL were determined as a function of distance down the tail. In addition, the effect of the entry process on energy spectra of protons and electrons in the magnetosheath and plasma sheet was determined.

The basic approach used for these calculations was to treat the entry and flow of plasma within the magnetosphere as a charged particle beam injection controlled by magnetic limiting currents. This approach and the expressions for the magnetic limiting currents were developed by C. L. Olson of Sandia National Laboratories using the qualitative gradient drift entry theory of *Olson and Pfitzer* [1985]. In this model the magnetosheath energy spectrum quantitatively determines the structure of the magnetosphere.

Section 2 of this document discusses in general the interaction of the solar wind with the magnetosphere, providing the background for the work performed in this study. Section 3 discusses the application of the GDE theory to quantitative modeling of the magnetosphere, including the essential aspects of the theory and the calculation procedure used. Section 4 discusses the results of the modeling, including the structure of

the LLBL, energy spectra of plasma within the magnetosphere, and current strengths within the plasma sheet; Section 5 compares the magnetic limiting currents derived under this study with currents measured in the magnetotail. Finally, Section 6 presents a summary of the results and discusses necessary work for the future.

Section 2

Interaction of the Solar Wind With the Magnetosphere

In order to understand the interaction between the solar wind and the magneto-sphere, it is first necessary to understand the characteristics of the plasma in the solar wind and the various regions of the magnetosphere. It is also necessary to understand the physical structure of the magnetosphere, including plasma regions, currents, and the magnetic field topology.

2.1 Solar Wind

The solar wind is highly variable, but energy spectra for both protons and electrons are described well by flowing Maxwellians. Typical parameters are a density around 10 particles/cm^3, a bulk velocity between 200 and 700 km/sec, and a temperature around 10 eV.

2.2 Magnetosheath

The magnetosheath is the region between the bow shock and the magnetopause. Here the shocked solar wind plasma flows around the magnetosphere. Typical plasma density in the magnetosheath is around 1 cm^{-3}, and typical bulk flow velocities are in the range of 100-400 km/sec. Plasma flow in the magnetosheath behaves much like the flow in a shock layer about a body immersed in a supersonic freestream: the density and temperature decrease with distance from the stagnation point, while the velocity increases.

Unlike the solar wind, energy spectra in the magnetosheath are not fit well by Maxwellian distribution functions. Instead, a kappa distribution [*Formisano et al.*, 1973; *Chan et al.*, 1975] has been found to fit the observed spectra well in many cases (see Appendix A for a description of the kappa-distribution). The kappa distribution has a

form similar to a Maxwellian at low energies (E<<kT) with an enhanced power-law tail at high energies. The kappa distribution becomes a Maxwellian in the limit as the parameter κ approaches infinity.

Proton and electron spectra differ considerably. Electrons [*Reiff and Reasoner*, 1975; *Eastman et al.*, 1985] do not seem to be fit well by a single sp ctrum. A two-component distribution must be used to fit the observed electron spectra, with a hot (kT ~ 100-400 eV), low density (n ~ 0.1 cm^{-3}) component superimposed on a cold (kT ~ 20-50 eV), high-density (n ~ 1 cm^{-3}) component. Electron spectra are generally seen to be fairly isotropic, but note that the characteristic thermal speeds are much higher than the proton bulk flow speeds. Protons [*Chan et al.*, 1975; *Eastman et al.*, 1985; *Williams et al.*, 1987] are characterized by flowing kappa distributions with bulk flow speeds around 100-400 km/sec and temperatures of 100-600 eV. As with the electrons, two-component distributions are often seen in proton spectra, both near the Earth [*Williams et al.*, 1987] and at lunar orbit [*Sanders et al.*, 1981].

2.3 Magnetosphere

Figure 1 shows a cross section of the magnetospheric tail, showing the major regions of plasma within the tail. Also shown in this figure are major current systems and directions of plasma flow in the tail. The tail of the magnetosphere may be divided into its plasma sheet and lobe regions. The plasma sheet is a region of relatively dense plasma which persists in the vicinity of the magnetic equatorial plane. The lobe regions, above and below the plasma sheet [*Williams and Mead*, 1965], by contrast, are almost devoid of plasma, and characterized primarily by their relatively strong magnetic fields which are directed toward the Earth (northern lobe) and away from the Earth (southern lobe). The magnetic field lines in the lobe regions are connected to the polar cap ionosphere. Similarly, those field lines that pass through the plasma sheet (and through the magnetic equatorial plane) are connected to the ionosphere just below the polar cap along the auroral oval.

In order to explain the lobe structure of the magnetic field in the tail, it is necessary

J

Lobe
Regions
With Very Low
Density Plasma

Return of
Cross Tail
Currents Just
Beyond Magnetopause

Magnetopause

E

Plasma Persists
Through Center
of Tail

Strong Boundary
Layer Electrostatic
Field Directed From
Dusk to Dawn Along
Both Flanks

J

Low Latitude
Boundary Layer
With Plasma
Flowing
Predominantly
in Anti-Solar
Direction

E

Electrostatic Field Across
Tail Directed From Dawn
to Dusk

J

Current
Flowing From
Dawn to Dusk
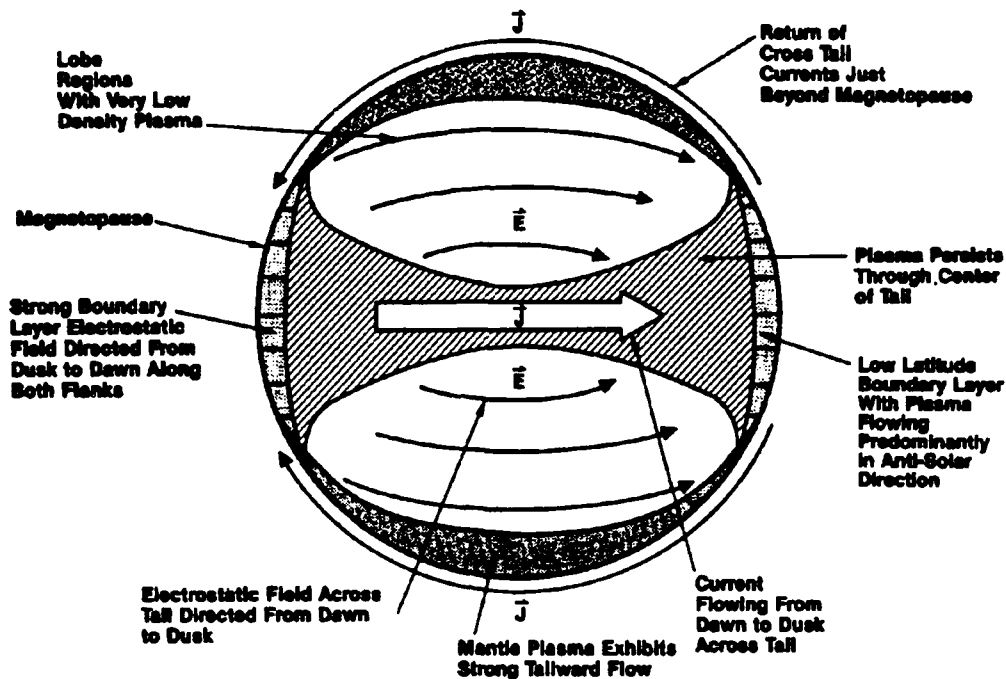Across Tail

Mantle Plasma Exhibits
Strong Tailward Flow

Figure 1.   Tail features that may be produced by magnetospheric response to charge buildup along the
flanks of the tail (except the mantle plasma which may be supplied by gradient drift entry in the
dayside cusp region.) From *Olson and Pfitzer* [1985].

to assume the existence of an electric current that flows from dawn to dusk through the
plasma sheet. These currents must return at or just beyond the magnetopause above
and below the lobe regions. The combined "theta" current forms two solenoids which
are responsible for lobe region magnetic field structure.

Currents also flow along magnetic field lines in the quiet magnetosphere [*Zmuda
and Armstrong*, 1974]. These field-aligned, or Birkeland, currents flow down to the
ionosphere on the dawn side of the magnetosphere and out of the ionosphere on the
dusk side [*Iijima and Potemra*, 1976]. Just below the latitudes where these "Region 1"
Birkeland currents connect to the ionosphere, a second field-aligned current system
exists; these are the "Region 2" Birkeland currents whose direction is opposite that of
the Region 1 currents.

The plasma sheet [*Hill*, 1974; *Chan et al.*, 1975] is characterized by lower number
densities ($n \sim 0.1\text{-}1.0$ cm^{-3}) and higher temperatures ($kT \sim 1\text{-}5$ keV for protons and 100-

500 eV for electrons) than the magnetosheath. Both proton and electron spectra are essentially isotropic. As with the magnetosheath, proton and electron spectra are fit well by kappa distribution functions. It is often observed that on average even during quiet magnetic conditions, plasma near the magnetic equator in the tail of the magnetosphere convects Earthward [Axford and Hines, 1961]. This motion requires the continuous presence of an electrostatic field directed from dawn to dusk across the tail, as is almost always observed [McCoy et al., 1975]. An electrostatic field, directed from dawn to dusk, is also present in the polar ionosphere and produces an antisolar flow of ionospheric plasma over the polar cap.

The low-latitude boundary layer is located just inside the magnetopause. Plasma flow is in the general antisolar direction. The flowing plasma has properties intermediate between the magnetosheath and the plasma sheet. Although much structure is seen the LLBL plasma parameters [Eastman et al., 1985a], the density and velocity are seen to decrease with increasing distance from the magnetopause, while the temperature increases. Plasma in the LLBL typically exhibits a strong flow tailward across the magnetic field. This plasma flow requires the presence of a strong electrostatic field directed from dawn to dusk (in the -y direction) along both the dawn and dusk flank of the tail (so that the $\underline{E} \times \underline{B}$ drift direction is tailward). This contrasts with the boundary layer (the plasma mantle) that persists just inside the magnetopause over the lobes of the tail where magnetosheath-like plasma is observed to flow tailward along magnetic field lines [Rosenbauer et al., 1975].

Eastman et al. [1976, 1985b] have identified the boundary layers, including the low-latitude boundary layer and the plasma sheet boundary layer, as the primary regions of transport of plasma and energy in the Earth's magnetotail. They found that the LLBL contributes directly to the low-energy component of the central plasma sheet. Thus an understanding of how plasma from the magnetosheath enters the LLBL and is transported across it is crucial to understanding the origin and development of the plasma sheet.

Section 3

The Gradient Drift Entry Model

3.1 Background

All early attempts to determine the shape and size of the magnetopause tacitly assumed that the solar wind particles incident on the magnetic field were reflected specularly and that therefore none of them permanently entered the magnetosphere. However, the assumption of specular reflection is only an approximation. The geomagnetic field at the magnetopause diminishes in total strength from about 75 nT at the subsolar point to less than 5 nT in the distant tail. Therefore a very small gradient in the magnetic field exists parallel to the magnetopause.

It is known that solar cosmic ray particles can enter the magnetosphere because they sample such a large region of the magnetosphere that the assumption of uniform magnetic field cannot be made [*Masley*, 1975; *Pfitzer*, 1979]. It is then natural to ask what is the lowest energy particle that can gain access to the magnetosphere because of gradients in the magnetic field.

The idea that low energy particles (~1 keV protons) can directly enter the magnetosphere has been suggested or implied by several authors [*Chapman and Ferraro*, 1930, 1932; *Vestine*, 1963; *Fejer*, 1965; *Wentworth*, 1965; *Stevenson and Comstock*, 1968; *Cole*, 1974; *Olson*, 1974; *Olson and Pfitzer*, 1974; *Bird*, 1975]. Recently, *Olson and Pfitzer* [1984, 1985] quantitatively studied the interaction of low energy (1-10 keV) ions and electrons with a realistic model of the geomagnetic field (one that contains gradients parallel to the magnetopause). They examined the motions of particles impacting at given locations on the magnetopause from various directions and found that, although particles with solar wind energies are deflected of the magnetopause for most directions of incidence, there exists an "entry cone" of allowed directions of incidence. Particles impacting at a point on the magnetopause within the entry cone can enter the magnetosphere. They found that the size of the entry cone (in steradians) is largest in the magnetospheric tail near the magnetic equatorial plane; entry essentially does not occur at angular distances greater than about 25° (about 6 R_E) off of the

geomagnetic equator. In addition, near the equator all particles moving in the anti-solar direction and making only small angles with respect to the magnetopause surface will gain entry. Due to the topology of the magnetic field, however, only protons and positive ions can enter on the dawn flank of the tail, and only electrons can enter on the dusk flank.

Olson and Pfitzer [1985] discussed some of the consequences of the gradient drift entry process. First, since the process occurs primarily near the geomagnetic equator, it provides a ready source of plasma to populate the plasma sheet. Particles with pitch angles near 90° will move across the tail; those with pitch angles near zero or 180° will move towards the ionosphere. Second, since protons move from dawn to dusk, and electrons move in the opposite direction, the net effect is a current near the equatorial plane in the dawn-to-dusk direction. The direction and location of this current is consistent with the cross-tail current known to flow through the plasma sheet. Third, because of the differential entry of protons and electrons, a charge separation will result, leading to an excess of positive charge just inside the dawn magnetopause and an excess of negative charge just inside the dusk magnetopause. This charge imbalance then creates a weak cross-tail electric field oriented from dawn to dusk through the middle of the tail, and strong dusk-to-dawn electric fields on each flank. The dusk-to-dawn electric field along the flanks is required to maintain the anti-sunward flow of plasma seen in the LLBL.

3.2 Magnetic Limiting Currents

In order to model the interaction between the magnetosheath and the magnetosphere, the entry of magnetosheath plasma has been treated as an injection of a charged particle beam [*Olson and Olson*, 1986]. The process is shown schematically in Figure 2. Two beams enter the magnetosphere along the equatorial flanks of the tail; a beam of protons and positive ions enters on the dawn side, and a beam of electrons enters on the dusk side. The mechanism for entry is the gradient drift process. Once inside the magnetosphere, the beams split into the Birkeland current, the plasma sheet current, and the tailward flow of plasma in the LLBL. The steady-state configuration is
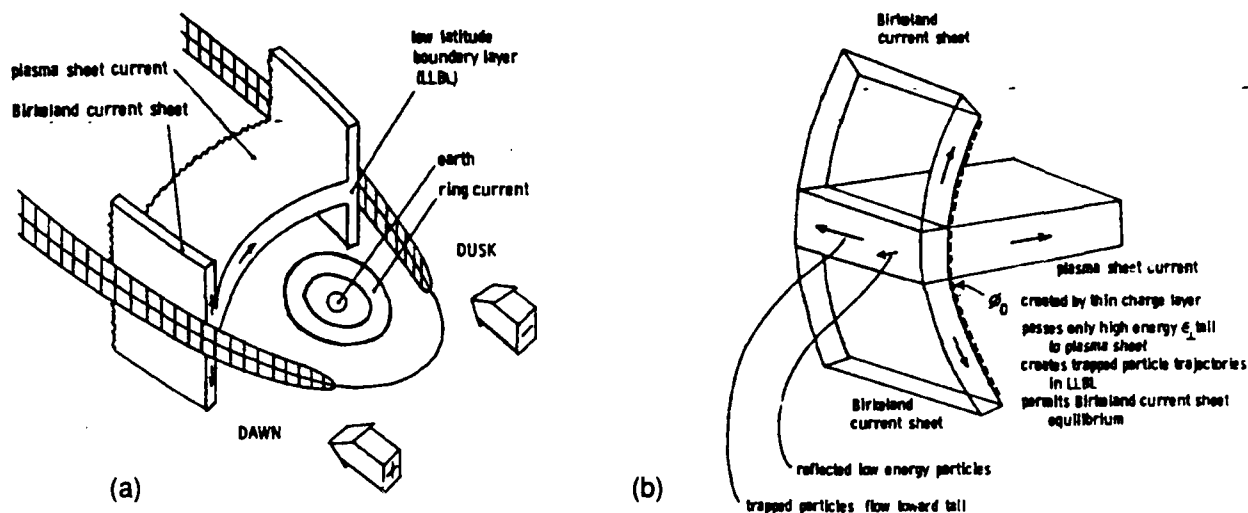
Figure 2. Gradient drift entry viewed as a charged particle beam injection. (a) A global view of the magnetosphere showing dawn and dusk flanks, low-latitude boundary layers, and plasma sheet. Protons (and positive ions) enter on the dawn flank, ans electrons enter on the dusk flank. (b) Steady-state configuration. A thin charge layer builds up on the inner edge of the LLBL, creating a potential difference ϕ_0. Some plasma can gradient drift across the LLBL into the plasma sheet, some travels along magnetic field lines from the LLBL to form the Birkeland region 1 currents, and some flows tailward within the LLBL.

shown in Figure 2b. A thin charge layer forms just earthward of the LLBL; this charge layer creates a potential, and consequently an electric field, across the LLBL. Magnetosheath particles with enough energy to cross this potential barrier (i.e., with energy W $>$ qϕ_{bi}, where ϕ_{bi} is the potential at the inner edge of the LLBL) can pass into the plasma sheet; they eventually drift across the magnetosphere and may pass out the other side. Particles with initial energies less than qϕ_{bi} cannot cross the potential barrier; their direction depends on their initial pitch angles. In this population, particles with pitch angles near 90 degrees drift tailward down the LLBL, while particles with pitch angles near 0 or 180 degrees drift along magnetic field lines and form the Birkeland currents.

The magnitude of the plasma sheet and Birkeland currents is limited by the magnetic field geometry [Olson and Olson, 1986]. The magnetic limiting current for a charged particle beam occurs when the magnetic field created by the current becomes large enough to turn the particles around and stop the propagation of the beam. Magnetic limiting currents have been derived for sheet current flow across the magnetic field (corresponding to the plasma sheet) and for sheet flow parallel to the magnetic field (corresponding to the Birkeland current). These magnetic limiting currents are

well-known within the particle beam community and have been experimentally observed and verified. The plasma sheet corresponds to a sheet flow of current across the magnetic field **B**, and the magnetic limiting current for this case is given by

$$J_{PS} = \frac{2B_0}{\mu_0 \sqrt{Lh_{PS}}}$$

where: J_{PS} = plasma sheet limiting current density (e.g., in amps/m^2)
B_0 = local magnetic field
μ_0 = permeability constant
   = $4\pi \times 10^{-7}$ weber/amp-m
L = magnetic field scale length
   = $\dfrac{B_0}{\nabla B_0}$
h_{PS} = plasma sheet thickness

The Birkeland Region 1 current system corresponds to sheet flow of current along the magnetic field vector and is given by

$$J_B = \frac{8}{\mu_0} \frac{m}{q\delta_{BL}^2} \frac{\langle v_{perp} \rangle^2}{\langle v_{par} \rangle}$$

where: m = particle mass
q = particle charge
δ_{BL} = LLBL thickness
$\langle v_{perp} \rangle$ = average particle velocity perpendicular to **B**$_0$
$\langle v_{par} \rangle$ = average particle velocity parallel to **B**$_0$

While there is bulk flow of plasma tailward down the LLBL, there is no net current, and hence no limiting current, in the LLBL. The primary drift motion is **E** x **B** drift due to the LLBL electric field, and electrons and protons drift in the same direction.

In the presence of an electric field across the LLBL, there is a minimum energy for which particles can enter and remain in the magnetosphere. In a uniform electric and magnetic field, a particle will trace out a cycloidal path which combines the circular

- 10 -

gyration due to the magnetic field and the $\underline{E} \times \underline{B}$ drift. For particles with energies less than

$$W_{crit} = \frac{2mE^2}{B_0^2}$$

the particle will be stopped at the cusp of the cycloid and will be reflected from the magnetosphere. Thus, some particles with initial directions which would allow them to enter and remain in the magnetosphere (without the electric field) will be reflected by the electric field. Corresponding to the critical energy W_{crit} is the critical potential $\phi_{crit} = W_{crit}/q$; this critical potential determines the maximum distance particles with energies less than W_{crit} can penetrate against the electric field. Knowing ϕ_{crit} and the potential at the inner edge of the LLBL, the boundary layer thickness ϕ_{bl} can be determined:

$$\delta_{BL} = \frac{\phi_{BL}}{B_0} \sqrt{\frac{2m}{q\phi_{crit}}}$$

3.3 Magnetosheath Model

Since the gradient drift entry process depends intimately on the energy spectrum in the magnetosheath, a model for the plasma properties in this region was required. In theory, measured energy spectra at various locations down the tail could be used, but in practice we are lucky to have a spectrum at one location. Sophisticated procedures are available to self-consistently determine the flowfield in the magnetosheath, e.g., *Spreiter and Stahara* [1980]. Since it was only necessary to compute the properties at the magnetopause, however, the approach used here was to use a measured spectrum at one location and use gas dynamic relations [*Howe and Binsack*, 1972] to determine the spectra expected at other locations. In order to specify the conditions at the magnetopause, it is necessary to know the solar wind Mach number M, the ratio of specific heats γ, and the local pressure p. By combining the normal shock and isentropic flow equations, the local density, velocity, and temperature can be determined for any point on the magnetopause.

The average value of the solar wind Mach number is about 8-10, with the vast majority of measurements between 6 and 12; for this study we have chosen a value of 10. (The flow parameters down the tail are fairly insensitive to the value chosen.) Typically, the ratio of specific heats is taken to be 5/3.

The major problem in determining the local properties along the magnetopause is determining the local pressure. If the shape of the magnetopause is known, the Newtonian approximation provides a reasonable value for the local pressure (see *Howe and Binsack* [1972] for the actual equations and their derivation).

Using these relations and given the Mach number in the solar wind, it is possible to scale the plasma parameters at one location to obtain the corresponding parameters at another location. Figures 3 through 5 show the calculated magnetosheath plasma properties assuming a solar wind Mach number M=10 and a ratio of specific heats γ=5/3 (the actual properties calculated are fairly insensitive to these parameters).
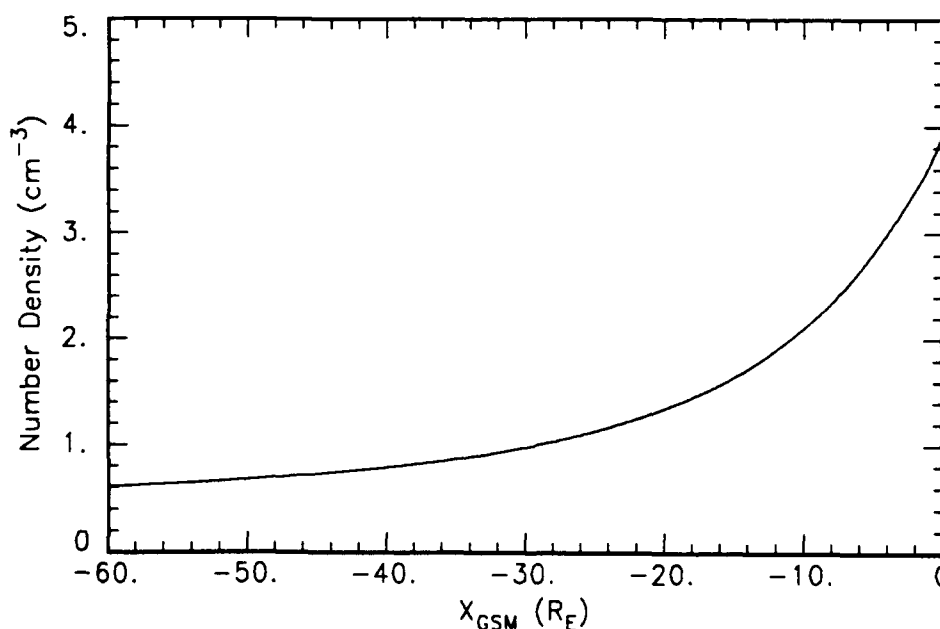
Figure 3. Variation of density within the magnetosheath using the gas dynamic model. Assumed freestream Mach number is 10.0, and ratio of specific heats is 5/3.
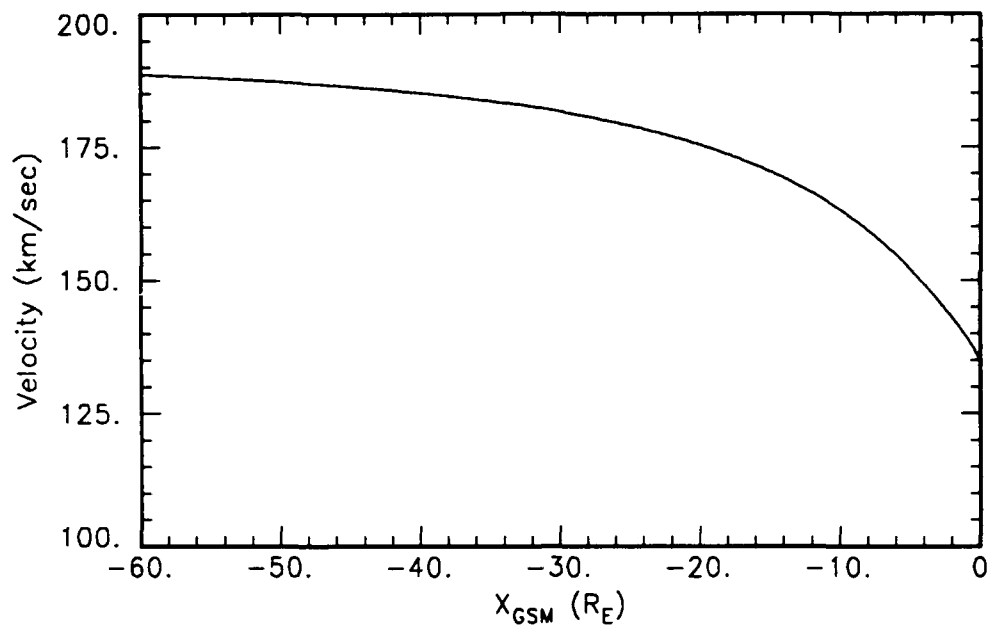
Figure 4.   Variation of velocity in the magnetosheath using gas dynamic relations.
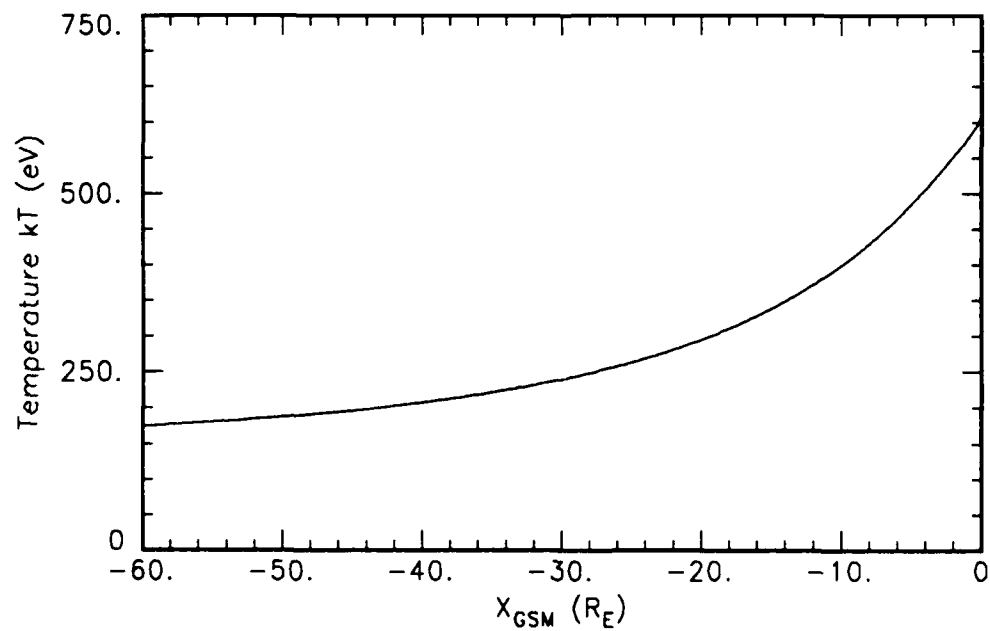

Figure 5.   Temperature variation in the magnetosheath using the gas dynamic relations.

3.4 Low-Latitude Boundary Layer Model

A model of the LLBL is used to obtain the potential and electric field within the LLBL. The model is two-dimensional, consisting of two plates infinite in the z-direction and separated by a distance δ. The inner plate corresponds to the inner edge of the LLBL, and the outer plate represents the magnetopause. The potential on the outer plate is fixed at zero, while the potential on the inner plate is set at ϕ_{bl}. Both δ and ϕ_{bl} are functions of x, the distance down the tail. The electric field $\mathbf{E}(x,y)$ is determined by taking the gradient of the potential ϕ.

3.5 Calculation Procedure

A typical energy spectrum for protons entering the magnetosphere is shown schematically in Figure 6. The curve shows omnidirectional flux versus energy; the area under the curve is the total flux of protons entering the magnetosphere (in this case with no LLBL electric field). The curve is divided into three regions. Particles with initial energy greater than $q\phi_{bl}$ have enough energy to pass completely across the LLBL and into the plasma sheet. Although ϕ_{bl} is not known a priori, we do know that the total current (or flux) across the plasma sheet is limited by the plasma sheet current J_{ps}, which we know from the magnetic field geome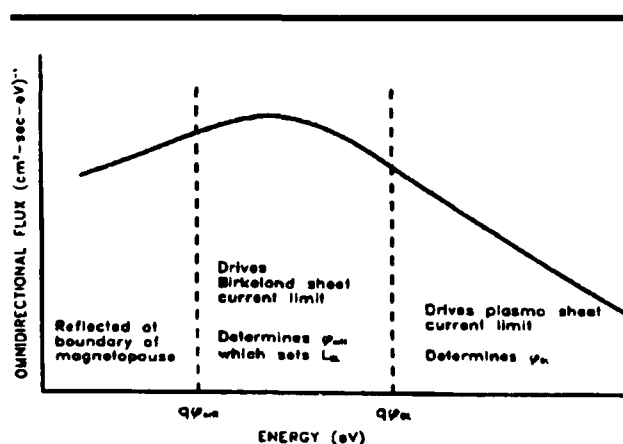try. Particles with energies less than $q\phi_{crit}$ are reflected at the magnetopause, and hence do not contribute to the magnetospheric current systems. Particles with intermediate energies populate the Birkeland current and the LLBL. Again, we do not know ϕ_{crit} a priori, but we do know that the total flux in this middle part of the spectrum must balance the Birkeland current and the tailward plasma flow through the LLBL. These observations lead to a calculation procedure which is discussed in detail in the

Figure 6. Population of current systems is determined by input energy spectrum in magnetosheath.

following paragraphs.

The first step of the procedure is to calculate the total omnidirectional flux j_i incident on the magnetopause using the measured magnetosheath energy spectrum. In order to simplify this step, an analytical representation of the magnetosheath spectrum is used. For this study, the magnetosheath spectrum was represented by a kappa distribution function.

The next step in the process is to assume models for the magnetospheric magnetic field ($\underline{B}$), the LLBL (thickness L_{bl} and potential ϕ_{bl}), and the plasma sheet thickness (h_{ps}). Present calculations use the quiet magnetic field model of *Olson and Pfitzer* [1974], assume initially that L_{bl} and ϕ_{bl} are zero (i.e., no LLBL electric field), and obtain h_{ps} knowing the latitudinal extent of particle entry on the magnetopause. These parameters are used to calculate the magnetic limiting currents J_B and J_{ps} using Equations (1) and (2). For subsequent iterations, the boundary layer thickness and potential calculated in the previous iteration are used.

Next, using the LLBL electric field model from Step 2, particle trajectory calculations are performed to determine the entry cone $\Omega(W)$ and the omnidirectional flux entering $j_c(W)$ (e.g., the curve shown in Figure 3).

The fourth step is to determine the boundary layer potential ϕ_{bl} by integrating $j_c(W)$ to balance the plasma sheet current. This is done by integrating backwards from infinity until the total flux (area under the curve) equals the flux corresponding to the limiting plasma sheet current:

$$j_{ps} = \frac{J_{ps}}{q} = \int_{q\phi_{BL}}^{\infty} j_c \, dw$$

where J_{PS} is the plasma sheet particle flux in $(m^2\text{-sec})^{-1}$.

The next step is to determine the critical potential ϕ_{crit} by integrating $j_c(W)$ to balance the Birkeland current and LLBL flow. This is done by integrating backwards from ϕ_{bl}

- 15 -

until the total flux equals the sum of the LLBL flux plus the Birkeland current flux:

$$j_{BL} + j_B = j_{BL} + \frac{J_B}{q} = \int_{q\phi_{crit}}^{q\phi_{BL}} j_c \, dw$$

where j_{BL} and j_B are the particle fluxes in the LLBL and in the Birkeland currents, respectively.

Next, we calculate the boundary layer thickness:

$$\delta_{BL} = \frac{\phi_{BL}}{B_0} \sqrt{\frac{2m}{q\phi_{crit}}}$$

Finally, using the new values for L_{bl}, we calculate the new limiting currents. Using the new values for L_{bl}, ϕ_{bl}, and ϕ_{crit}, we update the LLBL electric field model and go back to the third step, in which the particle entry calculations are performed. These calculations yield new values for the entry cone $\Omega(W)$. The other steps are then repeated to give new values for ϕ_{bl}, ϕ_{crit}, and L_{bl}, and the whole process is repeated until the currents balance and the LLBL structure does not change between iterations.

Section 4

Results

Using the theory and calculation procedures outlined in the previous section, the structure of the LLBL has been determined for a set of "representative" conditions. The objective of these calculations was to determine the thickness of the LLBL and the potential difference across the LLBL as a function of distance down the tail from approximately X_{GSM} = -10 R_E out to lunar orbit (X_{GSM} = -60 R_E). An additional objective was to predict the variation of the proton energy spectrum across the LLBL.

For these calculations, a data set from *Eastman et al.* [1985] was used; this data set has the advantage that proton and electron spectra were obtained in the plasma sheet and magnetosheath during a single traversal of the LLBL, covering a time period of about five hours. In addition, interplanetary and magnetospheric conditions were very quiet during this period; the daily sum of K_p was 87, which corresponds to an average value of about K_p=1. Kappa distribution fits were made to the proton and electron energy spectra; fitting parameters are listed·in Table 1 of Appendix A, and the proton spectra for the magnetosheath and plasma sheet are shown in Figure 7. These distributions were used as inputs to the GDE model described above. Since the data were taken at approximately X_{GSM} = 10 R_E, the gas dynamic magnetosheath model described above was used to scale the density, velocity, and temperature at other locations down the tail. The GDE model was then used to determine the structure of the LLBL and the effect on the particle spectra in the LLBL and plasma sheet.

4.1 LLBL Structure

The results of the self-consistent entry calculations using these computed magnetosheath properties are shown in Figures 8 through 11. Figure 8 shows the calculated proton fluxes in the plasma sheet and Birkeland current systems. The plasma sheet flux is identical to the uniform magnetosheath case, since the magnetospheric magnetic field topology is the same as in the previous case. The calculated proton flux in the
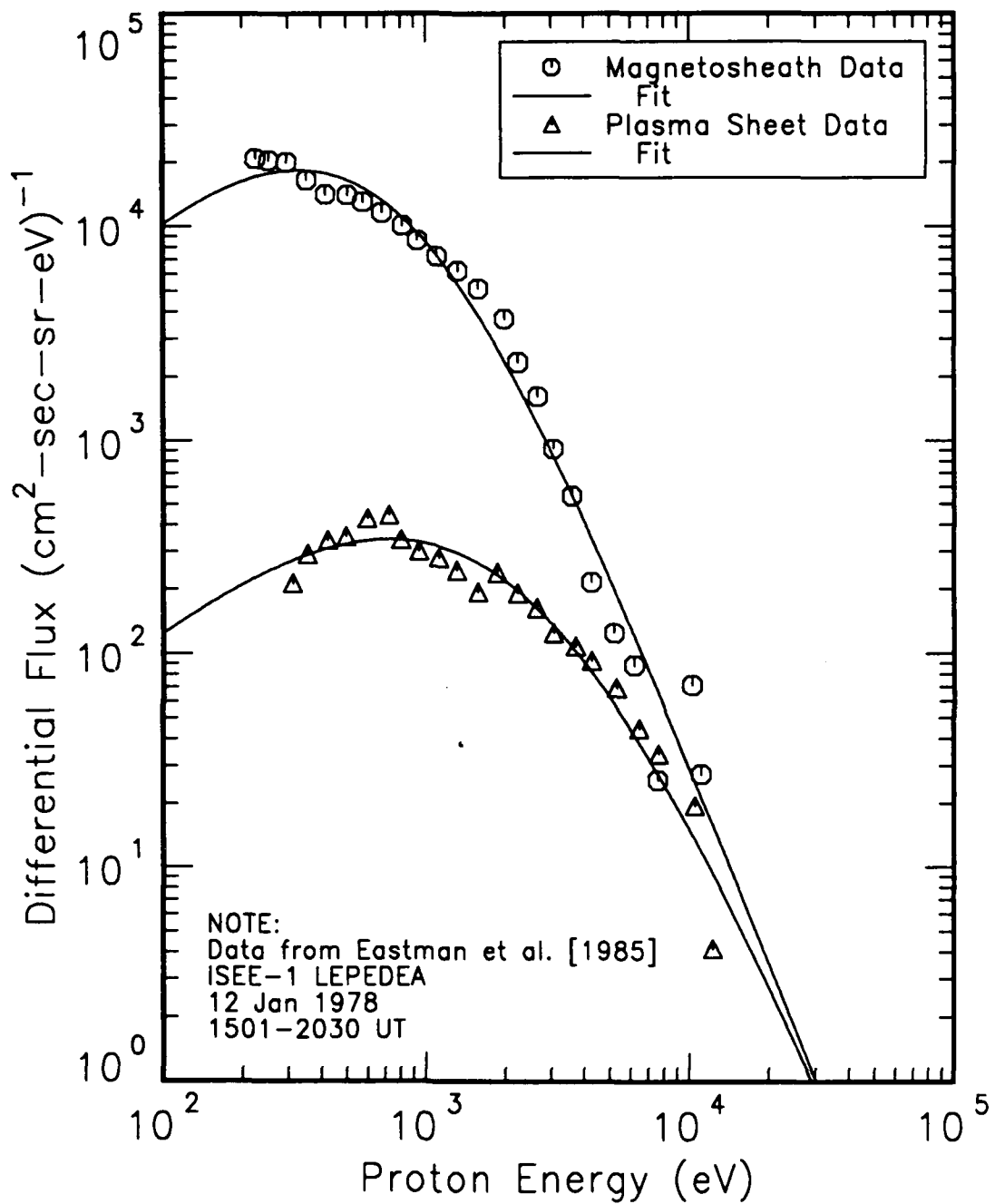
Figure 7.   Proton energy spectra in the magnetosheath and the plasma sheet measured by *Eastman et al.* [1985b]. Spectra were taken during a single pass through the LLBL by ISEE 1, covering a period of approximately five hours. Solid lines are kappa-distribution fits to the measured data.
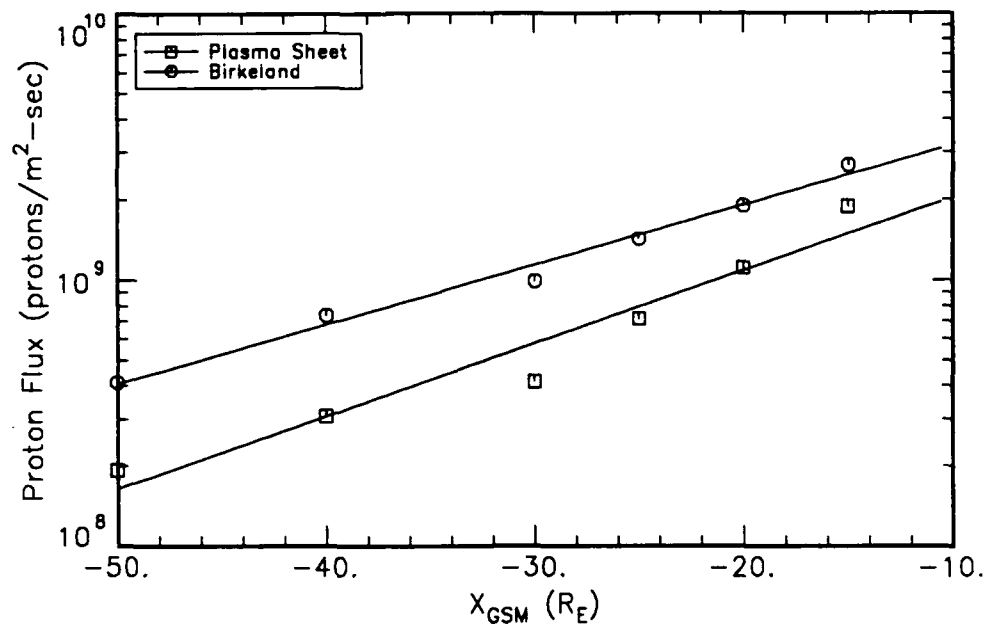
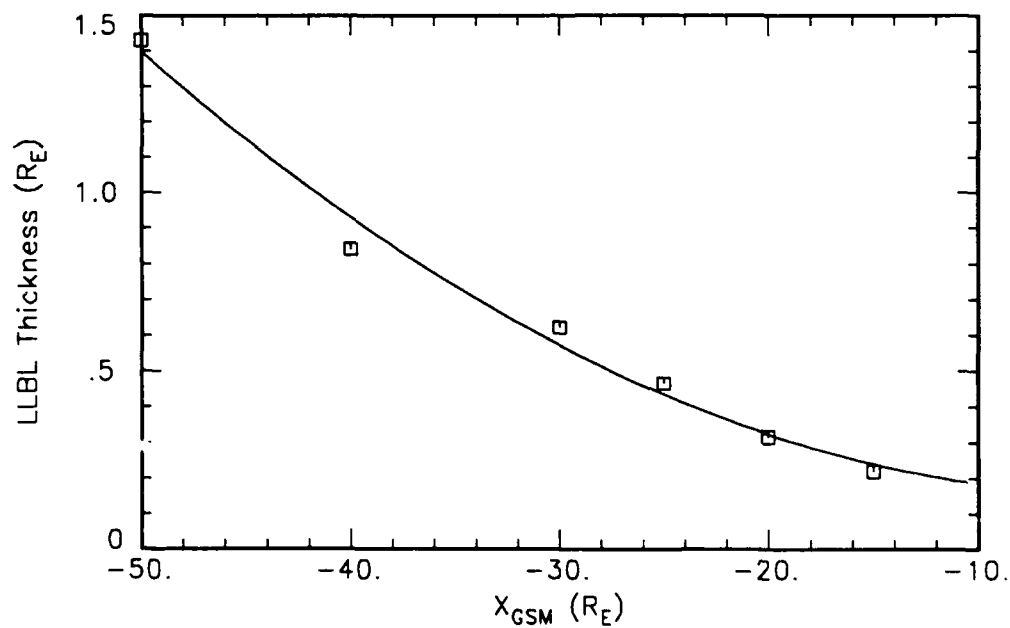Figure 8.   Calculated proton fluxes in the plasma sheet and Birkeland current systems.

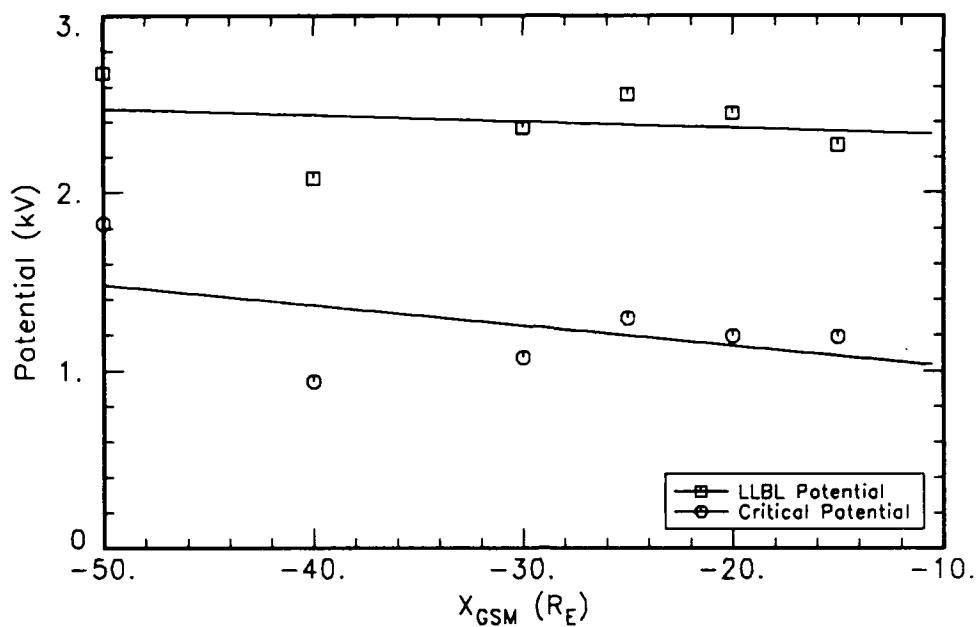Figure 9.   Calculated LLBL thickness.

Figure 10. Calculated potential at LLBL inner edge (ϕ_{bl}) and critical potential (ϕ_{crit}).
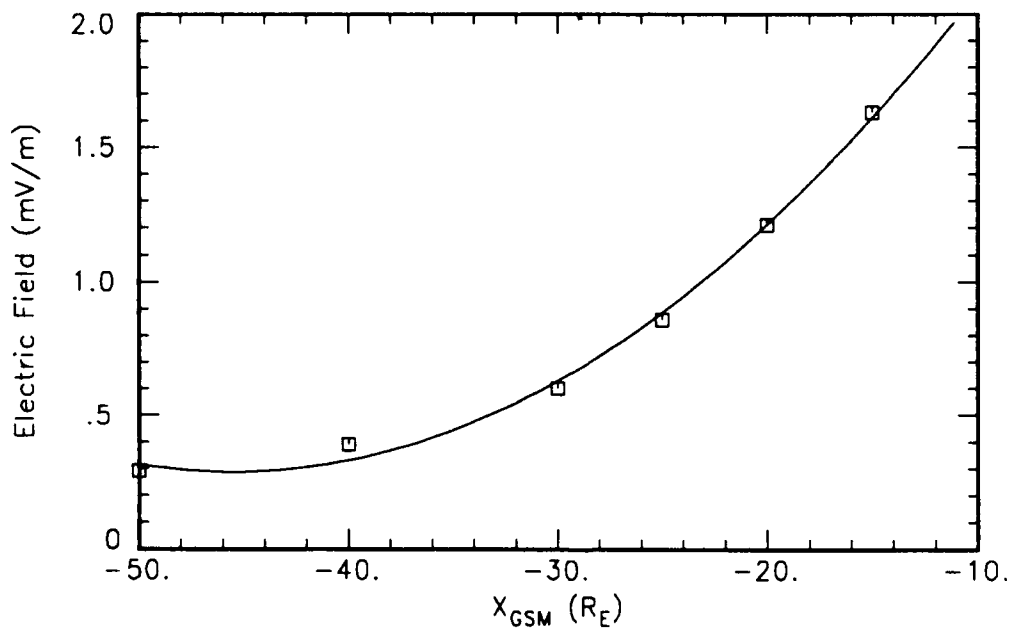

Figure 11. Calculated LLBL electric field.

Birkeland current system is slightly higher than in the previous case. The total proton flux in the plasma sheet is the same as in the previous case, 4.8×10^{24} protons/sec, and the proton flux in the Birkeland current system is 8.8×10^{24} protons/sec, compared with 7.7×10^{24} in the previous case. The equivalent currents are 7.7×10^{5} amps for the plasma sheet and 1.4×10^{6} amps for the Birkeland current.

Figure 9 shows the calculated boundary layer thickness, which increases from about 0.2 Earth radii at X=-15 to about 1.5 Earth radii at X=-50. The calculated thickness for the nonuniform magnetosheath properties is about the same as the previous case near thc Earth, but is about 25% less at larger distances.

The calculated potentials are shown in Figure 10. In this case the LLBL potential stays nearly constant with distance down the tail, ranging between about 2.0 and 2.8 kV. This behavior contrasts markedly with the rapid increase with distance down the tail seen in the case of uniform magnetosheath properties.

The calculated LLBL electric field is shown in Figure 11. The range of values is about the same as in the previous case (about 0.25 to 2.0 mV/m), but the electric field decreases more rapidly than in the previous case and then seems to level off at a fairly constant value beyond X=-40.

4.2 Energy Spectra

In order to provide further verification of the calculation procedures discussed above, the results of the LLBL calculations were used to predict the proton spectrum in the plasma sheet given the spectrum in the magnetosheath. The results are shown in Figure 12. The magnetosheath and plasma sheet proton spectra and fits are the same as shown in Figure 7. The dashed line is the plasma sheet spectrum predicted using the gradient drift entry model. The prediction agrees with the observed spectrum to within a factor of about two. The fact that the predicted spectrum is somewhat lower than the observed spectrum indicates that the actual LLBL potential was somewhat lower than the predicted 2268 volts. In general, however, agreement with the data is
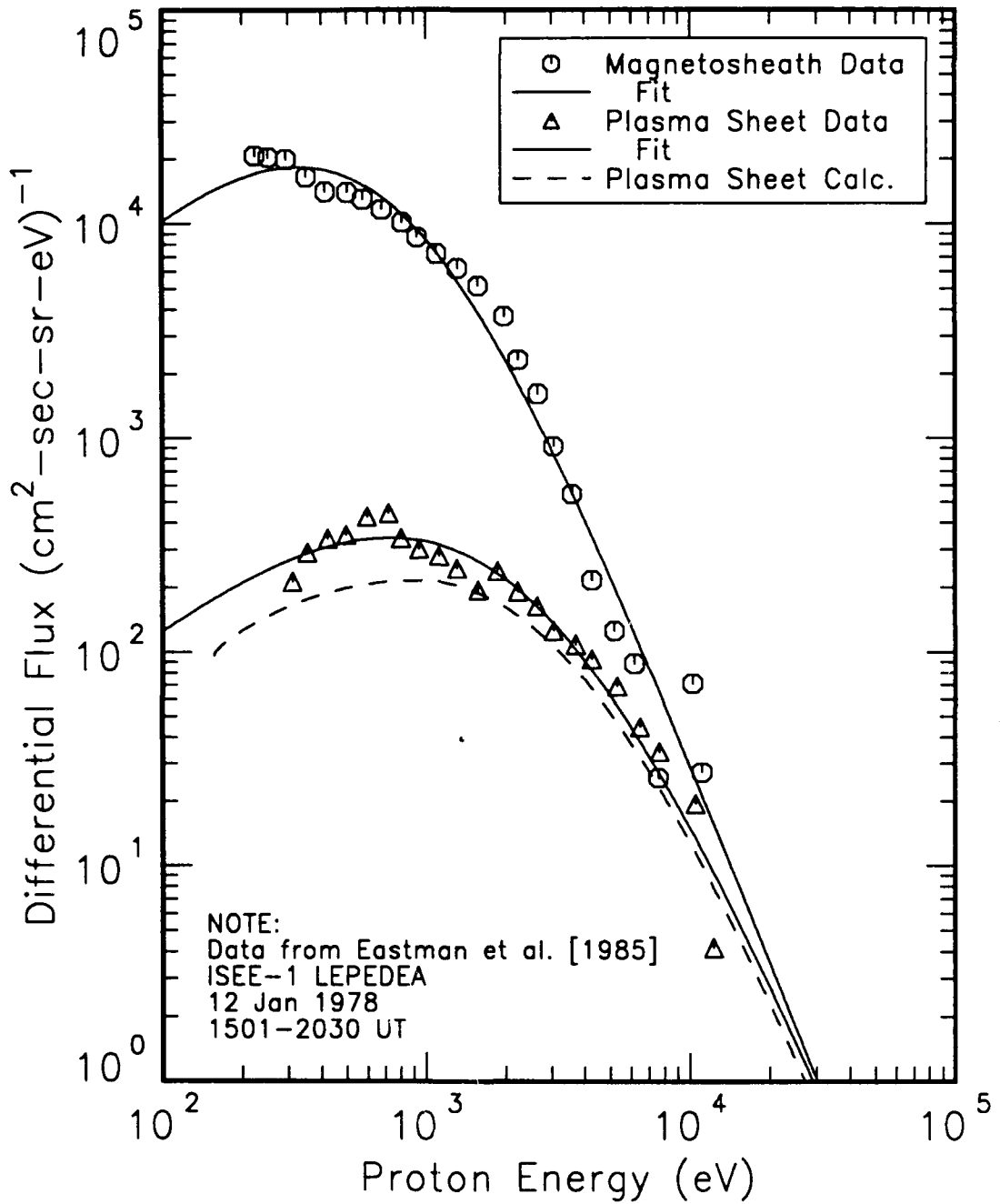
Figure 12. Proton energy spectra in the magnetosheath and the plasma sheet. The data points are measurements from *Eastman et al.* [1985b]; solid lines are kappa-distribution curve fits to the measured data. The dashed line shows the plasma sheet spectrum calculated using Gradient Drift Entry theory.

excellent, and confirms the fact that in the quiet magnetosphere plasma sheet protons have their source in the magnetosheath. The reduction in differential flux and apparent energization of the plasma is a result of the filtering action of the GDE process and the propagation across the LLBL potential difference.

In addition to protons entering from the magnetosheath and drifting into the plasma sheet, electrons will be able to gradient drift across the LLBL from the plasma sheet into the magnetosheath. Their spectra will also be modified by the protpagation acrosss the LLBL electric field. Figure 13 shows electron spectra reported by *Eastman et al.* taken at the same times as the proton spectra shown above. It can be seen that the magnetosheath spectrum is considerably lower than the plasma sheet spectrum at energies between about 200-2000 eV. Note also the enhanced flux above about 1000 eV in the magnetosheath spectrum. Also shown in the figure are spectra obtained by propagating the measured plasma sheet spectrum across various potential differences; it can be seen that the spectrum corresponding to a 1000 eV potential difference matches the high-energy portion of the magnetosheath spectrum quite well. Thus it appears as if the magnetosheath electron sr ...um consists of a low-energy component from the magnetosheath itself and a high-energy component which is made up of electrons which have drifted across the LLBL form the plasma sheet. This may be the explanation for the two-component spectrum seen in many magnetosheath electron measurements. It is not known at this time why the electron spectra are fit best by assuming a boundary layer potential of about 1000 volts, while the proton spectra are fit well by the calculated potential of about 2000 volts. Still, the fact that the two potentials agree within a factor of two is quite good at this stage.
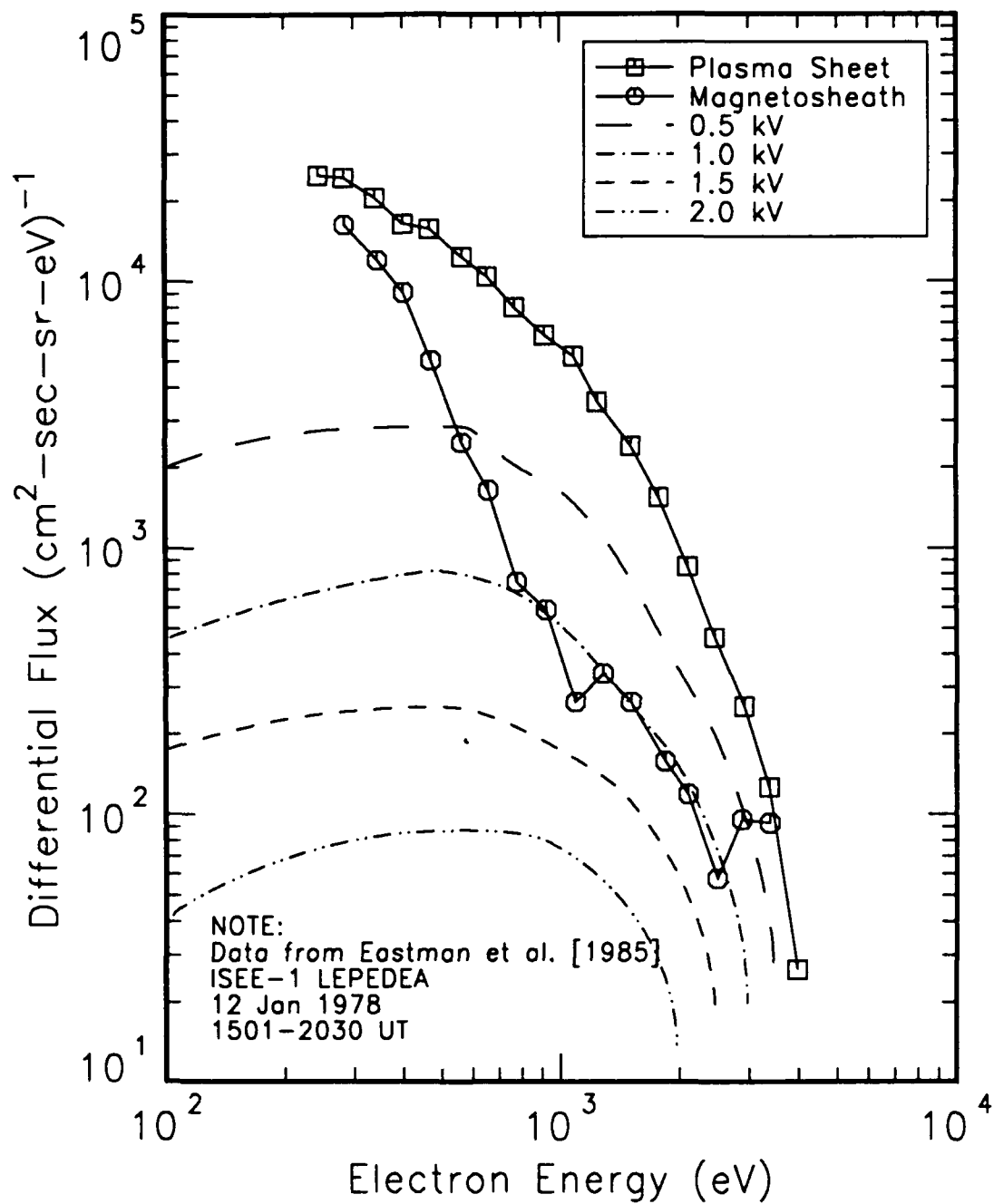
Figure 13. Electron spectra in the magnetosheath and plasma sheet. Data points connected by solid lines are measurements from *Eastman et al.* [1985b]. Dashed lines were calculated by propagating the measured plasma sheet spectrum across various potential differences, corresponding to electrons gradient drifting from the plasma sheet into the magnetosheath.

Section 5

Verification of Magnetic Limiting Currents

One of the cornerstones of the GDE theory is the concept of magnetic limiting currents discussed in Section 3. While these currents have been observed in laboratory experiments and are well-known within the charged particle beam community, verification on magnetospheric scales is desirable.

A recent study [*McComas et al.*, 1986] has used multiple-spacecraft observations by ISEE 1 and 2 to determine current sheet strengths in the magnetotail; these data were found to be useful for verifying the expressions for magnetic limiting current in the plasma sheet. In this section we compare current intensities calculated from the magnetic limiting current expressions with the experimentally derived values. In order to understand the comparison, it is first necessary to review the work of *McComas et al.*, including geometry, assumptions, and data analysis techniques.

5.1 Review of Experimental Data

In a recent paper, *McComas et al.* [1986] examine in detail three crossings of the near-tail current sheet by the ISEE 1 and 2 spacecraft on April 5, 1979. A unique aspect of these crossings is that the two spacecraft crossed the current sheet within about 30 minutes of each other, so that they were able to separate spatial and temporal variations quite well. The crossings occurred approximately 18 R_E tailwards of the Earth. In addition to the ISEE 1 and 2 spacecraft, ISEE 3 was monitoring the solar wind 220 R_E upstream of the Earth, and IMP 8 was in the near-Earth solar wind. The crossings were specifically selected to avoid times of large substorm activity. They thus provide a relatively idealized case in which to compare predictions of the GDE model with experimental data. The following paragraphs discuss the data, analysis techniques, and results presented in *McComas et al.*

The near-Earth magnetotail current sheet is an example of a field reversing sheet where two nearly anti-parallel portions of a magnetic field face each other. Prior to the launch of the coorbiting satellites ISEE 1 and 2, studies of current and plasma sheet topologies and dynamics have necessarily relied on data taken from single, or widely separated spacecraft. It is impossible for a single-spacecraft to separate spatial and temporal effects. Even with two-spacecraft observations, a fully three-dimensional geometry which might vary as a function of time, cannot be uniquely resolved. In this study, only current sheet crossings which exhibit planar, monotonic field variations were chosen. In addition to these constraints, the intersatellite separation vector must lie well out of the plane of the current sheet. Very fast sheet crossings were chosen in order to minimize the effect of temporal variations of the sheet structure itself. Since the geo-magnetic field in general, and the plasma sheet in particular, are subject to large and rapid variations as a function of substorm phase, current sheet crossings were specifi-cally chosen to avoid times of large substorm activity. Specifically, all three were chosen from a day when the variable pressure region behind an interplanetary shock caused large-scale motions of the magnetotail and repeated encounters between the current sheet and the ISEE 1 and 2 satellites. Bulk reorientations of the magnetotail due to variations in the solar wind flow, caused substantially enhanced geomagnetic activity on this day. Therefore, the crossings studied in the paper cannot be considered to be representative of "quiet" current sheet crossings. They do, however, probably represent crossings caused by bulk motions of the tail, and not internal, substorm-related recon-figurations.

5.1.1 Coordinate Systems

The coordinate system used in the paper for examining the sheet crossings is a local current sheet normal coordinate system. The current sheet is assumed to have surface boundaries which are planar and parallel on the size scale of the satellite separation vector. Magnetic field lines rotate through the current sheet so that fields on opposite sides of the sheet are roughly anti-parallel. The field rotation through the sheet is as-sumed to be symmetric about the current sheet midplane. The axis of symmetry is resolved from single-satellite magnetometer data alone. This axis is defined to be the

- 26 -

direction in which the field undergoes its maximum variance for the crossing, and is labeled as the L axis (which is close to the X_{GSM} axis).

Figures 14 and 15 show the field geometry. The N axis defines the current sheet normal, while the M axis lies in the plane of the sheet, completing the right-handed set. In the nominally expected magnetotail configuration, the L, M, N axes would correspond roughly to the GSM X, Y, Z coordinates, respectively. The L, M, N coordinates, however, describe a local coordinate system which may be quite different from the nominal configuration if the sheet surface is wavy, as has been suggested of the plasma sheet boundary, or if the tail becomes torqued around by the interplanetary magnetic field (IMF) B_y component. The magnetic field rotations are essentially confined to a plane, which is defined to be the L, n plane. In practice, the m and n axes are chosen so that the magnitudes of B_m and B_n are essentially zero and constant, respectively, through the crossing. The plane defined by the magnetic field rotation, as shown in Figure 14, may in general be inclined by the arbitrary angle, ϕ, with respect to the current sheet normal, N.
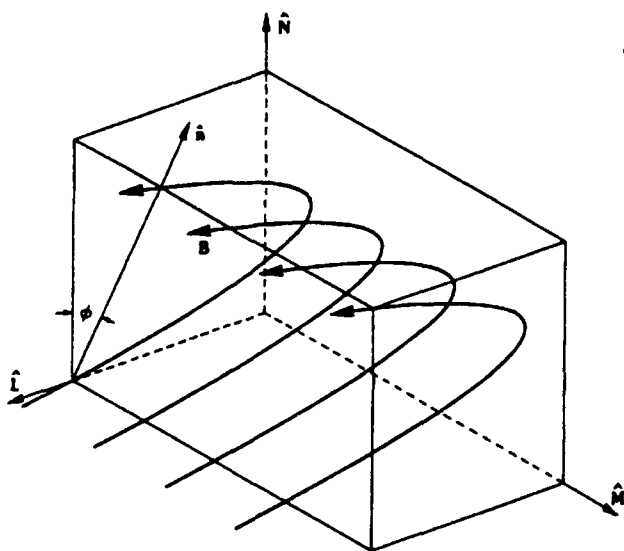

Figure 14. Magnetic field line rotations in the cross-tail current sheet. The planes of the field lines are inclined with respect to the sheet normal by the angle ϕ. The L axis bisects the field rotation, while current flows self-consistently in the M direction. From McComas et al. [1986].

For a current sheet with planar, parallel surfaces, as assumed here, only the component of the sheet motion perpendicular to the surface (in the N direction) is observable with intersatellite timing. In Figure 15, the geometry has been reduced to the plane, P, of the four coplanar vectors: M, N, m, and n. This is possible because the L axis is uniquely known, and motions of the sheet parallel to the L axis are unobservable with intersatellite timing, since the sheet is assumed to be uniform in the L direction. The m and n axes are also well known, but the arbitrary rotation angle, ϕ, is completely unknown. Since the normal to plane P, namely L,
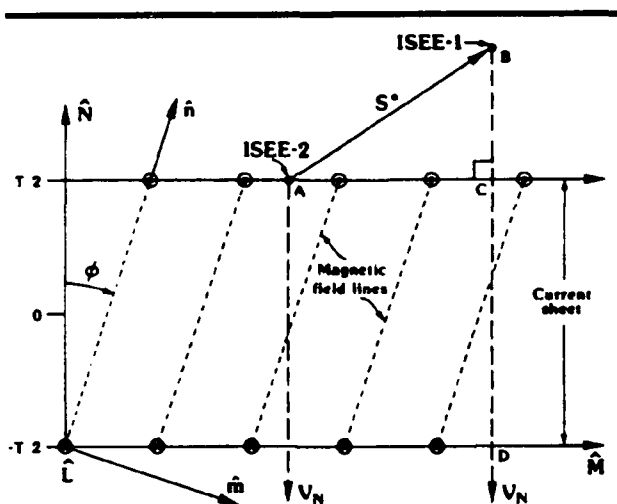
Figure 15. Cross-sectional cut through the current sheet in the plane perpendicular to the L axis. From *McComas et al.* [1986].

is well specified, it is possible to obtain the component of any known vector, **A**, in the plane. The general formula for the component of **A** in the plane, **A***, is **A*** = **L** x (**A** x **L**). This method is used in the paper, for example, to determine the component of the Z_{GSM} axis in this plane. The unit vector in this direction in the plane is called N_{NOM} as it represents the expected nominal direction for the sheet normal given that the X_{GSM} axis has been rotated to the L direction.

The component of the ISEE 1-2 separation vector which lies in the plane P, is labeled **S*** in Figure 15. **S*** is defined by **S*** = **L** x (**S** x **L**), where the separation vector, **S**, and the maximum variance axis, L, are both well specified. Only the compo-nent of the separation vector parallel to the *N* axis, $S_N = $ **S** · **N**, is used in determining the sheet normal velocity. If a constant normal velocity, V_N, is assumed, then this velocity can be determined by dividing S_N by the time lag, $\Delta\tau_{BC}$, between the initial encounters with the sheet seen at the two spacecraft (points B and C in Figure 15). The thickness of the sheet, T, is then simply the product of the normal velocity, V_N, and the duration of the crossing, $\Delta\tau_{CD}$. Figure 15 is drawn with the satellites moving in the *N* direction on the short time scale of the crossing. It is possible to calculate a maximum current sheet thickness for any crossing by finding the sheet thickness parallel to the arbitrarily ori-ented vector **S***. This is accomplished by letting $S_N = |$ **S*** $|$, since $S_N = $ **S** · **N** $< |$ **S*** $|$. This limiting thickness, T_{MAX}, would be highly variable, even if all current sheets were the same thickness, since the angles between **S*** and **N** are arbitrary. These thicknesses do, however, in all cases, set firm upper bounds on the actual sheet thicknesses.

5.1.2 Current Density

A detailed knowledge of the instantaneous current sheet normal velocity as a func-tion of time, through the crossing, is required to calculate the exact current density

distribution. This is because the current density is calculated from the curl of the magnetic field by Ampere's Law, curl $\mathbf{B} = \mu_o\mathbf{J}$. For the typical field geometry found in the near magnetotail, B_L is not a strong function of M, and both B_M and B_N have roughly constant, nonzero values. Since they are comparatively weak functions of the spatial coordinates, they do not contribute substantially to the curl of $\mathbf{B}$, and currents are driven essentially parallel to the m axis. The curl of the field in the L, M, N coordinate system is therefore simply $\mu_o J_M = \delta B_L/\delta N$, where δB_L and δN are replaced in practice by ΔB_L and $\Delta N = V_N\Delta t$, respectively. McComas et al. have developed a program to calculate the sheet normal velocity as a function of time assuming that all locations within the sheet and in the region of the crossing which have equal B_L magnitudes, occur at the same distance from the sheet midplane. This is equivalent to assuming that the sheet is constant in L and M on the size scale of the satellite separation vector, and does not change much on the intersatellite timing time scales. Since the separation vector is typically only a few thousand kilometers, and since the crossings are of short duration, typically a few minutes, this assumption is reasonable valid at all but active substorm times.

The magnetic signature of a typical quick current sheet crossing, which occurred between 1542 and 1556 UT on April 5, 1979, is shown in the upper panel of Figure 16. The magnitudes of B_{L2} at t_i and B_{L1} at t_j are equal by construction, as are the magnitudes of B_{L2} at t_j and B_{L1} at t_k. The time lags between the two points, t_{lag}, are simply $t_j - t_i$, and $t_k - t_j$, for the two periods, respectively. By similarly calculating t_{lag} at all times through the crossing, an approximately normal crossing velocity as a function of time can be deduced. The lower panel of Figure 16 shows the normal velocity profiles for the ISEE 1 and 2 spacecraft for the crossing.

5.1.3 Interplanetary Conditions

Just prior to 0200 UT on April 5, 1979, an interplanetary shock arrived at IMP 8 which was located in the solar wind in near-Earth orbit at approximately (-2, 22, 27) R_E in GSM coordinates. The IMF magnitude at this location rose from a value of 13 nT upstream of the shock to about 60 nT just downstream, and persisted until about 1500 UT when it began to drop back to the preshock value which it reached at about 2100
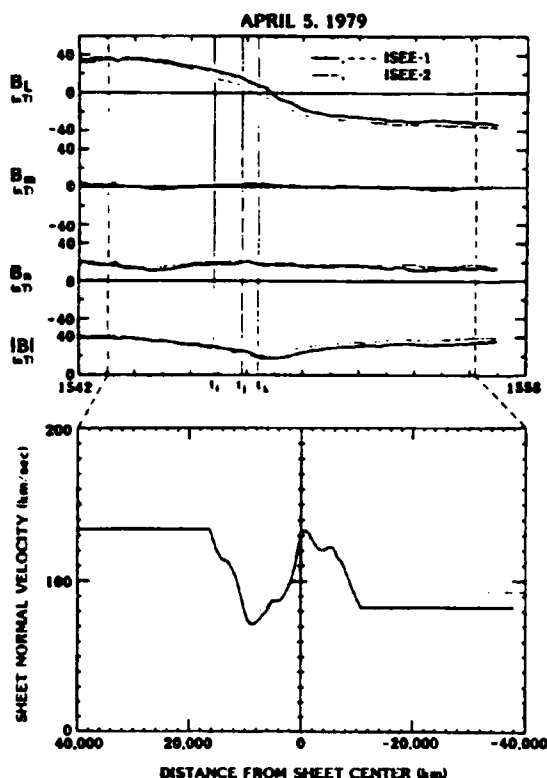
- 29 -

APRIL 5, 1979

Figure 16. Magnetic signature of the current sheet crossing which occurred at ~ 1550 UT. From *McComas et al.* [1986].

UT. *McComas et al.* report that the magnetic field observations suggest that the shock and related structures have spatial scale sizes sufficiently large to affect the magnetosphere as a whole. The downstream region is marked by numerous field rotations and variations in the total field strength. ISEE 3 data (not shown) indicate that the number density, and flow velocity are highly variable throughout the postshock region. The plasma pressure jumps across the shock by about a factor of 7, and is also highly variable ($P_{max}/P_{min} = 30$) throughout the day. These variations in flow direction and solar wind pressure cause substantial variations in the compression and orientation of the geomagnetic tail. On this day the coorbiting satellites ISEE 1 and 2, were traversing near the midplane of the geotail, and therefore in an ideal position to cross the tail current sheet. Reversals of the X component of the ISEE 2 magnetic field show that the current sheet was repeatedly encountered and crossed. From this set of partial and complete crossings, *McComas et al.* have chosen three particularly simple and interesting crossings. Rapid and smooth crossings of the geotail current sheet are relatively uncommon in the ISEE data sets, and are most often associated with geomagnetic storms and substorm activity. The crossings studied here were specifically chosen to be associated with bulk tail motions and not internal substorm-related tail configurations. The Z component of the IMF was approximately zero for 14 hours prior to the shock arrival and the AE index was small, indicating that the crossing at approximately 0200 UT was not due to a substorm. For the crossings at about 1515 and 1550 UT, the IMF had been substantially northward, indicating that substantial magnetic flux was not being added to the magnetotail, for at least 2 1/2 hours prior to each of these encounters. Such a time scale is sufficiently larger than the internal time scales of substorms that these crossings are probably not substorm related.

5.2 Comparison of GDE Model With Data

What follows now is a comparison of the cross-tail current density distributions measured by the ISEE 1 and 2 satellites and the ones obtained from the concept of magnetic limiting currents discussed in Section 3. To compute the magnetic field in the magnetotail, we have employed the Olson-Pfitzer dynamic magnetospheric magnetic field model. This model calculates the magnetic field contributions from the geomagnetic field, the magnetopause currents, the ring current, and the tail currents. Required inputs are the solar wind density and velocity, as well as the D_{st}. The fields in the magnetotail can be scaled to match disturbed conditions by varying a magnetotail so-called strength factor. The necessary solar wind input data are available from the NOAA CD–ROM optical disc, which contains solar wind and IMF data for the period 1963 to 1985.

The first crossing we will discuss occurred at 1550 UT. The top panel of Figure 16 shows the two satellite crossing signatures in their respective field line normal coordinate systems, as reported in *McComas et al.* The independently derived normals agree to within 8 degrees which indicates that the assumption of a simple, locally planar sheet geometry, is fairly good. At 1550 UT the satellites were located near the center of the magnetotail at (-17.6, -3.2, 0.2) R_E GSM (ISEE 1) with a separation vector **S** = (-6826, 1241, 2732) km, GSM. The L axes derived from minimum variance analysis are L_1 = (0.991, -0.008, 0.134) and L_2 = (0.975, 0.092, 0.202) for ISEE 1 and 2, respectively, in GSM coordinates. The small Y component of the L axes is reported as common for field lines near the center of the tail. The X and Z components indicate that the sheet is tilted upward toward the Earth by 8 and 12 degrees at the two satellites. The nominal sheet normals, N_{NOM}, for these L axes, calculated as described previously, are N_{NOM1} = (–0.134, 0.001, 0.991) and N_{NOM2} = (-0.201, -0.019, 0.979).

The current density profiles shown in Figure 17 were calculated by *McComas et al.* assuming these nominal sheet normals. While the absolute magnitudes of the current densities and thickness of the current peaks are a function of the choice of the sheet normal, the relative distribution of the features is not. The effect of choosing a different
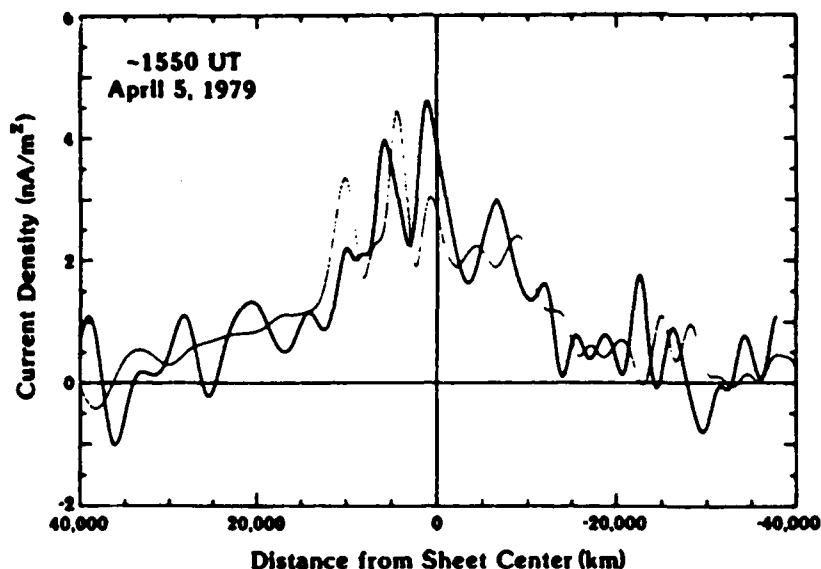
Figure 17. Cross-tail current density distributions for ISEE 1 and 2 displayed as a function of distance from the current sheet midplane for the crossing at ~ 1550 UT. From *McComas et al.* [1986].

current sheet normal is to inversely vary the calculated sheet thickness and current density magnitude. Since the total sheet current is fixed, a thicker sheet requires proportionally smaller current densities throughout the sheet.

For this particular crossing the geometry of the two satellites is fortuitous in that the separation vector between the satellites in the plane P, namely S^*, is only 22 degrees from the nominal normal. The maximum possible thickness, T_{MAX}, is therefore only 8% greater than the nominal thickness, T_{NOM}. This difference is of the order of other uncertainties in the calculation. Further, the field line normal, n, makes an angle of only 15 degrees with respect to N_{NOM}, and is toward S^*. This angle yields a thickness only 3% different from T_{NOM}, and is therefore even more negligible. Due to the unusually fortunate satellite/current sheet/field line geometry for this crossing, the calculated thickness and current density magnitudes are very likely to be correct.

The current density distribution shown in Figure 17 is comprised of two rather distinct regions. The majority of the sheet current is carried in a central structure which is approximately 25,000 km thick, and which is embedded in a larger region of somewhat smaller and more uniform current density. This broader region is approximately 70,000

km thick although the actual edges are not particularly well defined.

For the purpose of comparing the measured results with the model predictions, we integrated the current density over the sheet thickness, to get the current intensity in units A/m. The current density in Figure 17 was first digitized and subsequently integrated according to the trapezoidal rule to get the measure current intensity. Interplanetary magnetic field and solar wind data for April 5 were input into the Olson-Pfitzer model assuming a magnetotail strength factor of 1.0 in accordance with the quiet magnetic conditions. Based on the resulting values for **B** and Grad **B** in the current sheet, we integrated the magnetic limiting current with respect to sheet thickness to obtain the current intensity predicted by the MLC relations. This current intensity, as well as the ones measured by ISEE 1 and 2, are plotted in Figure 18, and the agreement between measured and predicted current intensity is excellent. One of the model assumptions is that the current sheet is centered at $Z_{GSM} = 0$, and since the satellites were located at Z_{GSM} = 0.2 for the 1550 UT crossing, we see that this is an accurate assumption.

The next crossing described by *McComas et al.* is the one at 0200 UT. An interplanetary shock arrived at the Earth just prior to 0200 UT on April 5, 1979, followed by
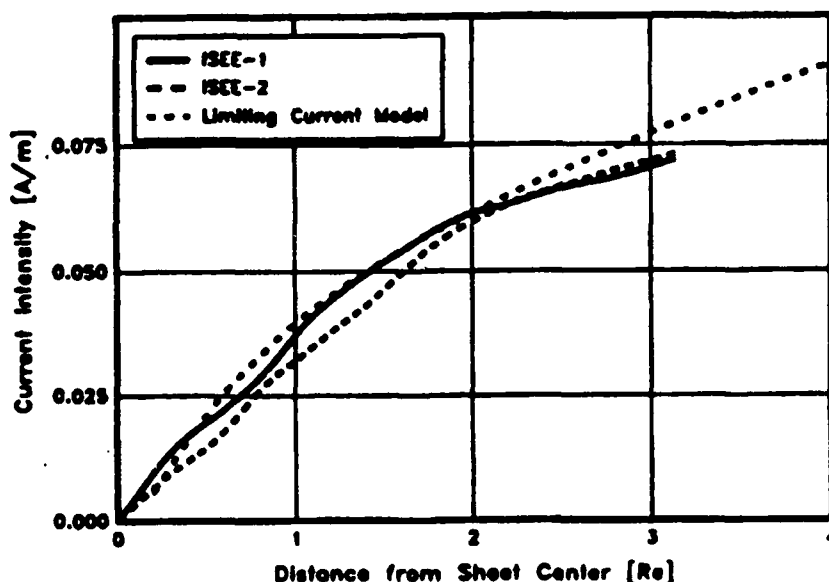

Figure 18. Plasma sheet current intensity calculated for the current sheet crossing at ~ 1550 UT, shown as a function of distance from the center of the current sheet. Also shown are the current sheet densities measured by the ISEE 1 and 2 spacecraft. Note the excellent agreement.

a region of enhanced plasma pressure. The current sheet crossing at about 0200 is almost surely a direct consequence of the initial impact of the interplanetary shock as it occurs at ISEE 1, about 22 R_E back in the tail, less than 10 min after the passage of the shock at IMP 8 (-2, 22, 27) R_E GSM. This yields an expected initial upward motion of the magnetotail. The crossing at the ISEE satellites is from the north to the south side of the sheet as would be expected for an upward tail motion. Figure 19 displays the magnetic field data, calculated normal velocity, and current density distribution for this crossing which occurred at (−22.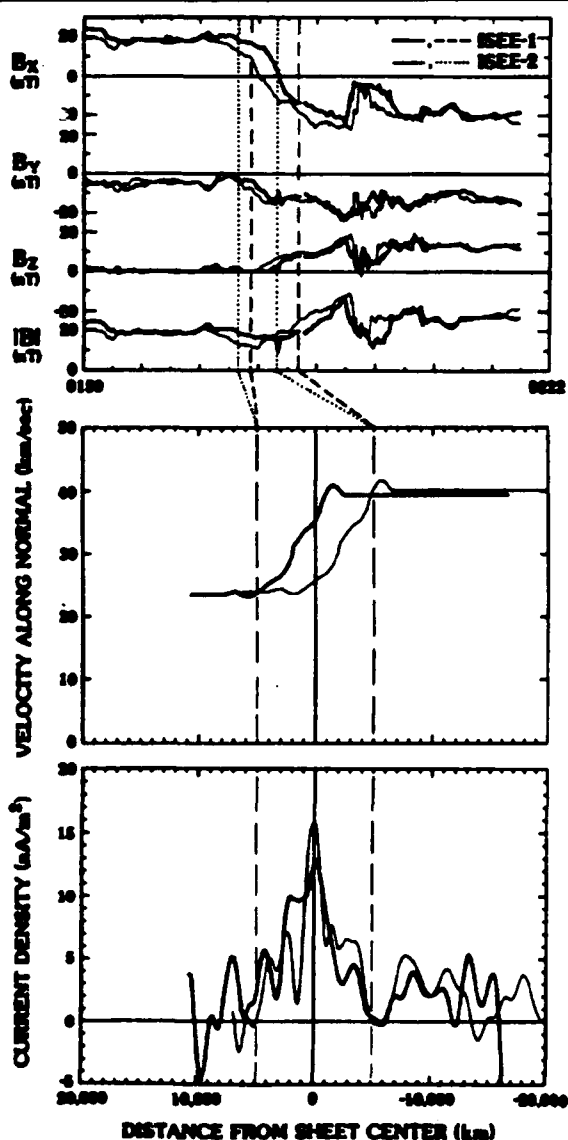0, −1.4, 4.0) R_E GSM (ISEE 1). The nominal normals were calculated by *McComas et al.* to be N_{NOM1} = (0.217, 0.052, 0.975) and N_{NOM2} = (0.197, 0.061, 0.979) and agree to within 4.4 degrees. The top panel shows the original magnetic field in the GSM coordinate system. The dashed vertical lines show which portions of the data correspond to the central region of enhanced current density in the bottom panel.

It is interesting to note the marked asymmetry in the magnetic field profiles. While the variation of the X component of the field is reasonable symmetric, the Y component decreases, and the Z component increases, both rather uniformly through the crossing. These profiles indicate that the magnetic pressure in the tail is increasing during the period of crossing as would be expected if the tail is being compressed by the arrival of the shock. In the lower panel, the current density calculated by *McComas et al.* is displayed. The thickness of the central enhanced region is about

Figure 19. Magnetic field, sheet normal velocities, and current density distributions for the crossing of ~ 0200 UT.

10,000 km, and the peak current density is in excess of 15 nA/m² at ISEE 2.

An interesting major difference between this case and the previous one is that the field lines in this current sheet have a large cross-tail component. The planes which contain the field line rotations, are in fact inclined by 74 and 71 degrees from the ISEE 1 and 2 most nominal normals, respectively. Magnetic field lines in this sheet crossing are therefore strongly directed in the cross-tail sense. The strong cross-tail component of the field in the sheet is from dusk to dawn ($-Y_{GSM}$). Geometries for the current sheet structures which are consistent with the observation of such a large field line inclination include a relatively nominal sheet orientation with highly inclined field lines in it, a sheet which is locally very wavy with reasonably perpendicular field orientations inside, or some intermediate configuration between these. It is extremely unlikely that the entire current sheet could be rotated by some 70 degrees this close to the Earth; however, it is possible that the sheet could be very wavy or lumpy and therefore could have sections which have locally inclined normals of 70 degrees or more.

The satellite separation vector for this crossing is (-573, 1503, 2389) km in GSM coordinates. The component of this vector in the plane normal to the L axis, S^*, becomes $S^* = (76, 1656, 2220)$ km. The scaling factor for the sheet maximum thickness and minimum current density is therefore only 1.2. This means that the greatest thickness that the nominally 10,000 km thick central structure could have is about 12,000 km, and the peak ISEE 2 current density must exceed 12 nA/m².

As with the previous crossing, we have integrated the measured current density over the sheet thickness. The current intensity as a function of sheet half-thickness is displayed in Figure 20. By inputting the appropriate solar wind data into the Olson-Pfitzer magnetospheric model, we obtained the **B** and Grad **B** values needed to calculate the magnetic limiting sheet current; the latter was subsequently integrated with respect to sheet thickness. This result is compared to the current intensities derived from *McComas et al.* calculations in Figure 20. Although the cases agree to within a factor of 2-3, the excellent agreement seen in the previous crossing is no longer present. This result will be discussed in the next subsection.
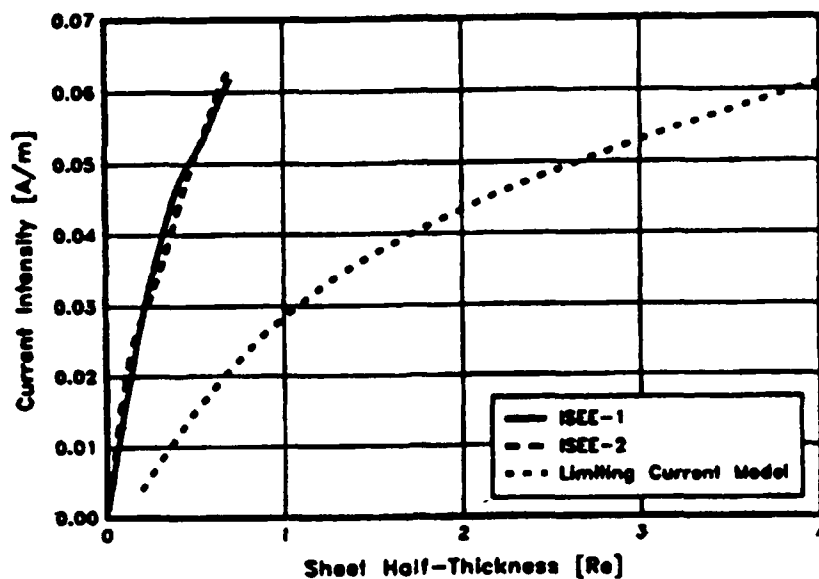
Figure 20. Comparison of measured and calculated current sheet intensities for the crossing of ~ 0200 UT.

The last April 5, 1979, crossing studied occurred at about 1515 UT at (-17.9, -3.1, 0.4) R_E GSM (ISEE 1). The crossing carried the satellites from the northern to the southern side of the sheet as shown in the top panel of Figure 21. Sheet nominal normals derived independently for the two satellite data sets agree to within 5.2 degrees, again indicating a locally flat sheet topology. The bottom panel displays the *McComas et al.* calculated current sheet current densities as a function of location in the sheet, under the assumption of the nominal normal, as for the previous examples. Again, a relatively narrow current density peak is observed in the center of the sheet. The thickness of this structure is approximately 10,000 km thick, and the peak current is more than 50 nA/m². This value is appreciably larger than those measured for the previous two examples, but the full sheet thickness is also narrower than previously observed.

Field line derived axes yield normals which are rotated from the nominal normals (−0.152, -0.018, 0.988) and (-0.178, -0.038, 0.983) to directions of (0.019, -0.845, 0.535) and (0.079, -0.877, 0.471) or through angles of 57 and 61 degrees for ISEE 1 and 2, respectively. The B_y component of the field is small, but in a sense inconsistent with the expected sense of the IMF at the time of this crossing. Calculation of the maximum sheet thickness based on the orientation of the separation vector in the sheet, S*, yields a thickness which is only 20% larger than that derived for the nominal normal.
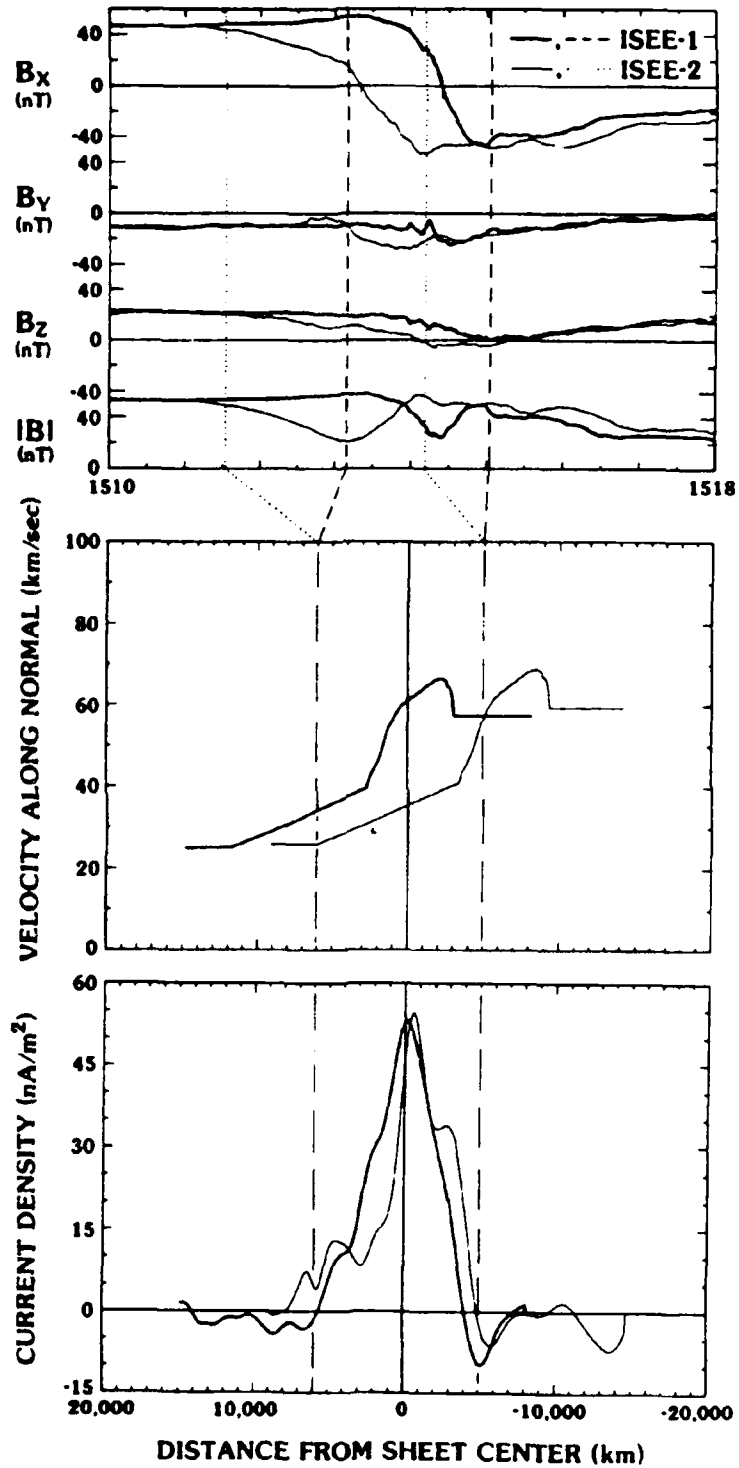
Figure 21. Measured magnetic field, normal velocity, and current density for the crossing at ~ 1515 UT.

The firm upper bound on the current sheet thickness for this case is therefore only 12,000 km.

The integrated magnetic limiting current intensity for this case has been calculated from the Olson-Pfitzer magnetospheric model, and is plotted together with the current intensities derived from the *McComas et al.* data in Figure 22. The measured and predicted current intensities agree to within a factor of about 5, as opposed to the nearly perfect agreement displayed in the 1550 UT crossing.

5.3 Discussion

As we have seen, the MLC model produced excellent agreement with one of the cases measured by *McComas et al.*, but was only within a factor of about five of the measured current intensities for the other two cases. This subsection will discuss some
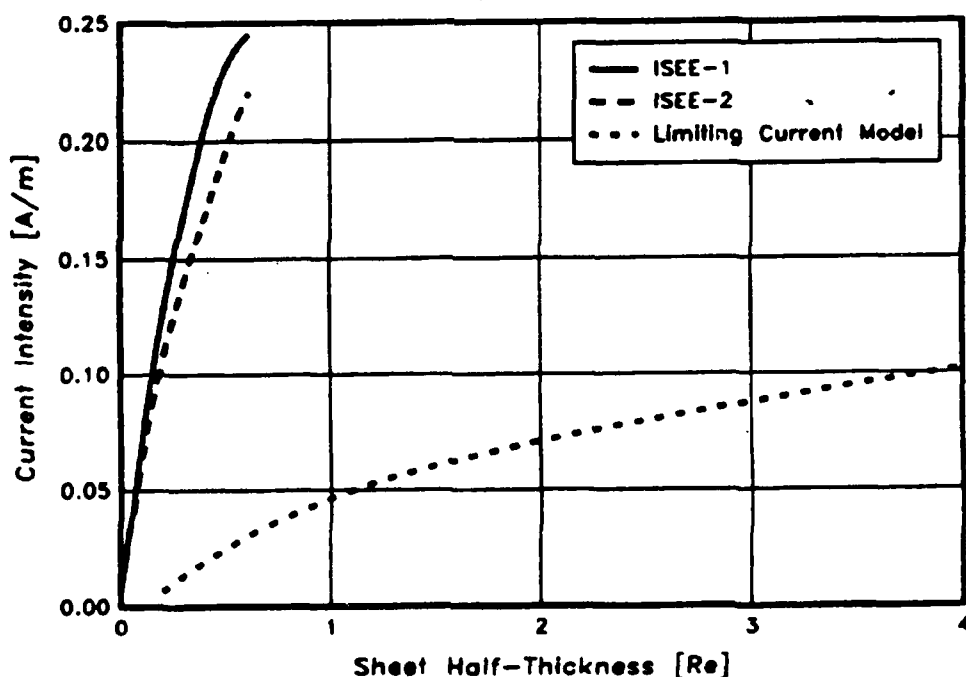

Figure 22.   Comparison of calculated and measured current intensities for the crossing of ~ 1515UT.

of the reasons for the discrepancies.

As *McComas et al.* mention, the 1550 UT calculated thickness and current density magnitudes are very likely to be correct due to the unusually fortunate satellite/current sheet/field line geometry. This is also the case for which the magnetic limiting current (MLC) model predicts current intensities in total agreement with the ones derived from the ISEE data. The 0200 and 1515 UT crossings are characterized by substantially tilted (> 60 degrees) field lines with respect to the current sheet nominal normal. Since the entire day of April 5 was devoid of magnetic substorm activity, it is not clear why such large inclination angles would occur. The interplanetary shock which drives the current sheet up and down with respect to the ISEE 1 and 2 satellites might be playing a role. One explanation offered [*Moses et al.*, 1985] suggests that oppositely rotating convection patterns of the open field lines in the two polar caps can cause motion of the closed (plasma sheet) field lines which are in the sense to shear the sheet, and create large cross-tail magnetic field components in the plasma sheet. Even without knowing what causes the field line inclination, it is clear that the tilted configuration represents an abnormal situation in the magnetotail. The electrodynamic forces required to distort the nominal field line configuration must include substantial electric currents in addition to the nominal plasma sheet current. The Olson-Pfitzer dynamic magnetospheric model is not designed to include such abnormal currents, and it is therefore unreasonable to expect the model to predict the actual magnetic field in this case.

It seems plausible that the extreme current densities reported for the 0200 and 1515 UT crossings are related to the large inclination angle of the magnetic field lines. If all three crossings had occurred at nominal conditions, one would expect that the current densities (in A/m²) integrated over the respective thicknesses of the current sheet would result in similar current intensities (in A/m). However, when comparing Figures 18, 20, and 22, this is clearly not the case since the 1515 UT crossing current intensity is 3-4 times greater than the others. The excess current must be related to the inclination of the magnetic field lines.

We also investigated changes to the inputs of the Olson-Pfitzer magnetic field model in order to improve the agreement with the data. These modifications took two forms: adding the IMF to the local field predicted by the Olson-Pfitzer model, and increasing

- 39 -

the tail strength factor.

There is a consensus in the community that the IMF, carried by the solar wind, can enter the magnetosphere and add to the local magnetic fields there. The manner in which this happens is, however, still not totally clear. According to work being done by MDSSC for the Office of Naval Research (ONR), the IMF can enter the magnetosphere in the form of electromagnetic waves, and the wave B_z component would be superimposed on to the local magnetic field. The entire day of April 5, 1979 (as well as the previous day) was characterized by low magnetic activity in the solar wind. If the IMF B_t component is included in the MLC calculation for the 0200 UT crossing ($B_t = 14.12$ nT), the computed sheet current intensity increases by only about 25%, which still leaves the MLC current intensity well below the ones derived from *McComas et al.* Only when the IMF contribution was increased to 500 nT did the MLC model match the data; this value is obviously unrealistic.

The Olson-Pfitzer magnetospheric magnetic field model allows the user to simulate magnetically disturbed conditions in the magnetotail by varying a so-called magnetotail strength factor. Nominally, this factor is set to one, but at disturbed conditions it can be increased to two. Even though the solar wind data for April 5 does not indicate such disturbed conditions, we have investigated how sensitive the magnetic fields are to this factor. When the strength-factor-two local magnetic fields are input into the MLC calculation, the original sheet current is increased by about 100%. This is expected since the MLC current is proportional to the square root of the magnitude of both the magnetic field and the field gradient. However, the MLC current is still less than 50% of the currents derived from the results in *McComas et al.*

In order to see what magnitude magnetic fields are required to match the sheet current derived from the 1515 UT ISEE data, we computed the magnetic limiting current intensity for a magnetotail of strength factor two, and various IMF B_t components added. Only when the IMF contribution was increased to a totally unrealistic field strength of 500 nT did the MLC model match the ISEE data. Figure 23 shows the effects of increasing the strength factor and adding an IMF B_z of 500 nT.
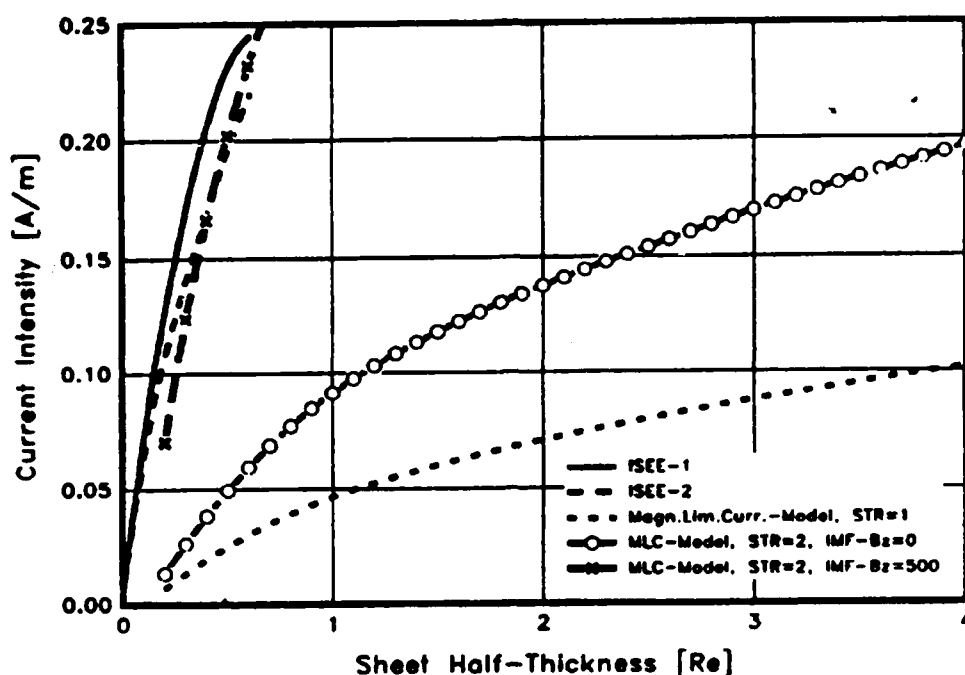
Figure 23. Comparison of measured currents with predictions for the crossing of ~ 1515 UT. Predictions include effects of increaing the tail strength factor and adding an assumed IMF B_z=500 nT.

Recall that the magnetic limiting current was proportional to the square root of both the local magnetic field, as well as of the gradient of the local field. By introducing the effect of the severely inclined field lines into the magnetic limiting current calculation, an increase in **B** is achievable. Sheet currents derived from both of the crossings (0200 and 1515 UT) which the MLC model was unable to reproduce, were both characterized by extremely inclined (57 to 74 degrees with respect to the GSM ZX plane) magnetic field lines. Thus, even though the current sheets were relatively thin for these two cases (about 10,000 km), the values of **B** at the upper and lower sheet edges correspond to the **B** values at the edges of a nominal "uninclined" thicker current sheet. Figure 24 illustrates this effect. Now, since the Olson-Pfitzer magnetospheric model assumes a nominal magnetotail current sheet, perpendicular to the GSM Z axis, with uninclined field lines, the effect of the tilted field lines is not captured. The effect can be captured by manipulating the location of the sheet edges. As Figure 17 shows, the current sheet can be made nominal by rotating the field lines by 74 degrees (largest ISEE inclination) towards the GSM Z axis. The Olson-Pfitzer model will obviously give different magnetic field values at points A and B in Figure 24. So when the magnetic limiting current density is integrated over the current sheet thickness, the sheet thickness shouldn't be 2 R_E as in *McComas et al.*, but rather be adjusted to the corresponding nominal field thick-
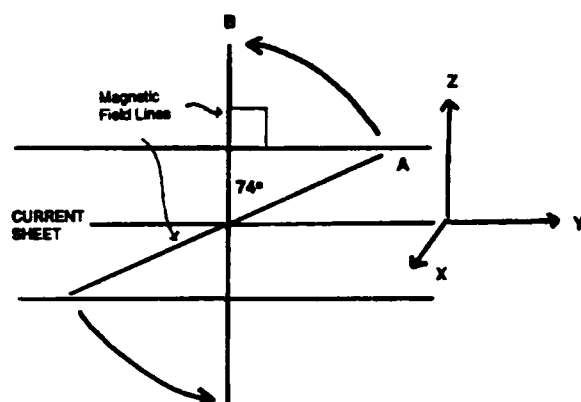
- 41 -

Figure 24. Tilting of magnetic field lines with respect to current sheet normal.

ness which is proportional to the reciprocal of the cosine of the inclination angle.

In the 0200 UT case, inclination angles of 71 and 74 degrees are reported. For an angle of 74 degrees, the adjusted nominal sheet thickness would be $1/(\cos 74°) = 3.6$ times larger than the 1 R_E reported in *McComas et al.* The magnetic X component at the sheet edge then increases from about 40 nT (70 nT) to about 70 nT (130 nT) for a magnetotail strength factor of 1 (2). Since the magnetic limiting current is proportional to the square root of **B**, this would amount to an increase in MLC current intensity of about 35%. For the 1515 UT case and an inclination angle of 61 degrees, the corresponding increase is about 25%. In neither case is this sufficient to match the ISEE-derived current intensities, but we are getting closer.

As described previously, *McComas et al.* used Ampere's Law to derive sheet currents from the measured magnetic field. Due to the magnetic field topology, they simplified Ampere's Law to $\delta B_L/\delta N = \mu_o J$, where $\delta B_L/\delta N$ corresponds roughly to $\delta B_x/\delta Z$ in GSM coordinates. Without having access to the detailed current calculations of *McComas et al.*, it is still possible to obtain a coarse $\delta B_x \delta Z$, and hence the sheet currents, by graphically estimating the gradient of B_x with respect to Z in Figures 21 and 23. The maximum gradients in B_x are observed at the center of the current sheet, and that is where we will perform our estimates. The estimates can then be compared to the current densities calculated by *McComas et al.* to make sure their results are consistent.

For the 1550 UT crossing we estimate the B_x gradient to be about 350 nT/80,000 km, or about 4.4×10^{-6} nT/m. Through Ampere's Law, this amounts to a current density of approximately 3.5 nA/m², which compares well to the 4.5 nA/m² shown in *McComas et al.* This is the crossing for which the magnetic field lines are basically nominal, and where our MLC model matches the ISEE derived results perfectly.

For the 0200 UT crossing, Figure 19 gives a B_x gradient of about 70 nT/10,000 km,

- 42 -

or 7×10^{-6} nT/m. This supports a current density of 5.5 nA/m², which is well below the about 13 nA/m² shown in *McComas et al.* Finally, looking at the 1515 UT crossing, Figure 21 indicates a B_x gradient of approximately 350 nT/10,000 km, or 3.5×10^{-5} nT/m. According to Ampere's Law, the current density is then 27.9 nA/m², substantially below the about 53 nA/m² presented in *McComas et al.* Hence for the two crossings whose current intensities we were unable to reproduce with the MLC model, we have detected at least a factor of 2 discrepancy between the current densities based on the graphical gradient of B_x in the L direction, and the current densities calculated by *McComas et al.*

Let's assume that the current densities we calculated from the graphically derived magnetic field gradients, are correct. This allows us to reduce the previously derived ISEE current intensities by a factor of about 2. Furthermore, by including the effect of inclined field lines, we showed that the MLC current intensities can be increased by about 25 to 35%. This certainly leads to some interesting results. Figure 25 shows the 0200 crossing. First, the MLC current has been increased 33%, corresponding to a magnetic field line inclination of 74 degrees. Now, if we finally add the effect of the IMF B_z (14.12 nT at the time) , we see that the MLC current intensity matches the ISEE data perfectly! Figure 26 shows the modified 1515 UT crossing. The ISEE current intensities have been reduced 50%, and the MLC current intensity has been increased 25%, corresponding to a field line inclination of 61 degrees. The MLC intensities are plotted for both quiet magnetic conditions (magnetotail strength factor = 1) and disturbed conditions (strength factor = 2). The IMF B_z was too small at the time (about 0) to make a difference. The match between ISEE and MLC current intensities is not as good as for the 0200 UT crossing, but we have managed to decrease the difference from a factor of about 8 to a factor of about 3.
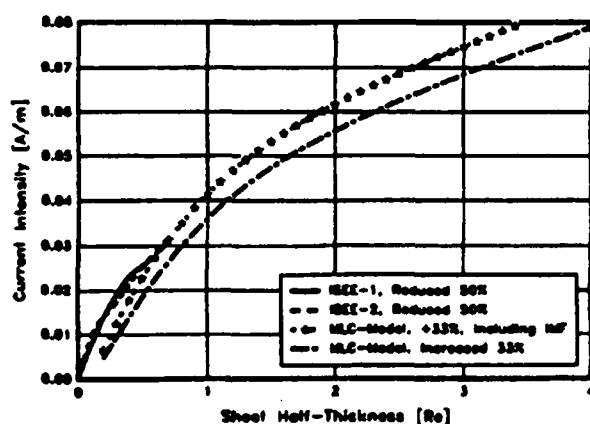
Figure 25. Predicted and measured current intensities for the crossing of ~ 0200 UT.

Thus, for the first plasma sheet crossing presented by *McComas et al.*, agreement between the calculated magnetic limiting current and the measured current is nearly perfect. For the other two crossings discussed, the

Figure 25. Predicted and measured current intensities for the crossing of ~ 1515 UT.

agreement may be quite good, but direct comparison between measured and calculated values is difficult. Possible explanations for the discrepancies include the contribution of the IMF to the local field; inclination of the magnetic field lines leading to inaccuracies in the data analysis technique used by *McComas et al.*; possible inaccuracies in their data analysis; and local currents which cannot be reproduced by a global magnetospheric model. Still, the agreement is encouraging. Futher verification of the model through comparison with other available current sheet crossings is desirable. Both magnetically quiet, as well as disturbed conditions should be simulated.

Section 6

Summary and Conclusions

A great deal of progress has been made under this contract. Beginning with the basic knowledge of the gradient drift entry process developed during our previous work, we have developed the GDE theory to the point where we can now determine the structure of the magnetosphere and the plasma properties within the magnetosphere given only the properties of the magnetosheath. This has been accomplished by treating the GDE process as a charged particle beam propagation problem controlled by limiting currents. Magnetosphere parameters determined include:

o Magnetosheath flux entering the magnetosphere

o LLBL thickness and electric field

o Magnitudes of the plasma sheet and Birkeland currents

All of the parameters calculated agree with observations. The comparison with the current sheet measurements of *McComas et al.* [1986] provides further verification of the concept of magnetic limiting currents in the magnetosphere.

We have also been able to predict plasma properties within the magnetosphere (the LLBL and the plasma sheet) given the magnetosheath energy spectrum and a model of the LLBL. Properties determined include the energy spectrum (flux and phase space density), density, bulk flow speed, and temperature. We are also able to determine profiles of these properties across the LLBL. Again, the calculations agree well with observations.

Many of the qualitative predictions of the GDE process were discussed in *Olson and Pfitzer* [1985]. One of the primary predictions was that the process operates at virtually all times and thus can explain features which are observed at all times in the magneto-sphere (such as the plasma sheet and the Birkeland current systems). Another major point was that the process allows entry of plasma near the locations where it is observed in the magnetosphere; i.e., plasma enters primarily in the equatorial region of the flanks of the tail, which is where the plasma sheet is located. Thus, no complicated

transport process is required to get the plasma from the point where it enters to the location where it is observed. Finally, the process explains the directions of the currents and electric fields found within the magnetosphere, as shown in Figure 1.

The work performed on this contract has extended these qualitative predictions to provide quantitative predictions of the flux of particles entering, the strength of the plasma sheet and Birkeland current systems, the thickness of the LLBL, and the magnitude of the LLBL electric field. The primary input to these calculations was a measured energy spectrum from the magnetosheath. These calculations were performed self-consistently in that the single-particle entry calculations used a model for the LLBL which was based on the magnetic limiting currents within the magnetosphere. The calculations used the quiet magnetospheric magnetic field model of *Olson and Pfitzer* [1974]. To be totally self-consistent, the magnetic field could have been calculated from the calculated currents within the magnetosphere, but in practice the *Olson and Pfitzer* model already provides a realistic model of the magnetospheric magnetic field.

The calculated particle fluxes agree with estimates and observations. *Hill* [1974] estimated that an entry flux of approximately 10^{25} to 10^{26} particles/sec was required to balance known loss mechanisms operating in the magnetosphere. Our calculation for the total proton flux entering was 1.3×10^{25} protons/sec, near the lower range of *Hill's* estimate, but recall that our test case involved a fairly low magnetosheath density and very quiet interplanetary and magnetospheric conditions, so that a low entry flux would be expected.

Measurements of the LLBL thickness are difficult because bulk plasma motions are difficult to separate from spacecraft motions in single-spacecraft observations. Available data indicate, however, that thicknesses on the order of a few tenths to several Earth radii are typical in the tail [*Hill*, 1974; *Eastman et al.*, 1976]. *Mitchell et al.* [1987] report that the LLBL thickness increases with distance from the subsolar point. Our calculated LLBL thickness is consistent with these observations, increasing from about 0.2 R_E at X_{GSM}=-10 to about 1.4 R_E at X_{GSM}=-50 R_E.

Our calculated LLBL potential and electric field are also consistent with

observations. *Mozer* [1984,1986] reports average LLBL potentials of 2.5 to 3.1 kV, with only a few cases above 6 kV. Our model calculated a value of about 2.5 kV; this potential remained essentially constant with distance down the tail. The electric field determined by the GDE model varied from approximately 2 mV/m at X_{GSM}=-10 to about 0.3 mV/m near lunar orbit. In an extended study of the LLBL out to X_{GSM}~-20 R_E, *Mitchell et al.* [1987] report values ranging from 3 to 5 mV/m, with 10 mV/m being the maximum value observed.

Finally, the ability of the model to duplicate the observed proton spectra in the plasma sheet is striking. To our knowledge, this is the only model which can predict the change in energy spectra across the LLBL. The model thus resolves the question set forth by *Hill* [1974] regarding the origin of the plasma in the plasma sheet and the method by which it is accelerated. The work performed on this contract demonstrates conclusively that the plasma sheet consists primarily of plasma from the magnetosheath which has entered the magnetosphere by the gradient drift entry process. The plasma continues to drift across the LLBL, with gradient drift providing the driving force required to transport the plasma against the LLBL electric field. The drift across the potential barrier acts as a high-pass filter mechanism which only allows particles above a certain energy access to the plasma sheet. The flux of these particles is reduced according to Liouville's theorem. Thus GDE provides a simple mechanism for the energization and reduction in flux observed. There is no need for a two-step process as proposed by *Hill*.

Thus we have shown that the GDE process accounts for many of the observed features of the magnetosphere. No other theory known to us can account qualitatively or quantitatively for these features.

The next step beyond this effort would be to perform similar calculations for other interplanetary conditions. The calculations performed under this contract were done for only one interplanetary state. The next step will be to perform similar calculations for other interplanetary states. This will allow us to further validate the computational techniques and also will improve our understanding of how the magnetosphere responds to changes in the solar wind. For example, how do the LLBL thickness and potential respond to increases in the density, temperature, and velocity of the solar

wind? A considerable body of experimental data exists to perform these verification calculations. For example, *Mitchell et al.* [1987] list a number of ISEE crossings of the LLBL; many of these crossings could be used. It may also be possible to use data from the IMP-8 spacecraft and the particle detectors placed on the moon during the Apollo program. The major requirements for the theory in its present form is that the magnetosphere must be in a relatively "quiet" state; i.e., interplanetary conditions must be varying slowly, and the IMF should be small and preferably northward-pointing.

Section 7

REFERENCES

Axford, W. I., and C. O. Hines, "A Unifying Theory of High Latitude Geophysical Phenomena and Geomagnetic Storms, " *Can. J. Phys.*, **39**, 1433, 1961.

Bird, M. K., "Solar Wind Access to the Plasma Sheet Along the Flanks of the Magnetotail," *Planetary and Space Science*, **23**, 27, 1975.

Chan, K. W., D. M. Sawyer, and J. I. Vette, "A Model of the Near-Earth Plasma Environment and Application to the ISEE-A and -B Orbit," NSSDC/WDC-A-R&S 77-01, July 1977.

Chapman, S., and V. C. A. Ferraro, "A New Theory of Magnetic Storms," *Nature*, **126**, 129, 1930.

Chapman, S., and V. C. A. Ferraro, "A New Theory of Magnetic Storms," *Journal of Geophysical Research*, **37**, 147, 1932.

Chen, F. F. *Introduction to Plasma Physics*, New York, Plenum Press, 1974.

Cole, K. D., "Outline of a Theory of Solar Wind Interaction With the Magnetosphere," *Planetary and Space Science*, **22**, 1075, 1974.

Coleman, P. J., Jr., "A Model of the Geomagnetic Cavity," *Radio Science*, **6**, 321, 1971.

Eastman, T. E., E. W. Hones, Jr., and J. R. Asbridge, "The Magnetospheric Boundary Layer: Site of Plasma, Momentum and Energy Transfer From the Magnetosheath Into the Magnetosphere," *Geophysical Research Letters*, **3**, 685, 1976.

Eastman, T. E., and E. W. Hones, Jr., "Characteristics of the Magnetospheric Boundary Layer and Magnetopause Layer as Observed by Imp 6," *Journal of Geophysical Research*, **84**, 2019, 1979.

Eastman, T. E., B. Popielawska, and L. A. Frank, "Three-Dimensional Plasma Observations Near the Outer Magnetospheric Boundary," *Journal of Geophy ical Research*, **90**, 9519, 1985a.

Eastman, T. E., L. A. Frank, and C. Y. Huang, "The Boundary Layers as the Primary Transport Regions of the Earth's Magnetotail," *Journal of Geophysical Research*, **90**, 9541, 1985b.

Fenner, M. A., and J. W. Freeman, "Dawn-Dusk Magnetosheath Plasma Asymmetries at 60 R_E," *Journal of Geophysical Research*, **80**, 3693, 1975.

Formisano, V., G. Moreno, F. Palmiotto, and P. C. Hedgecock, "Solar Wind Interaction with the Earth's Magnetic Field 1. Magnetosheath," *Journal of Geophysical Research*, **78**, 3714, 1973.

Hardy, D. A., P. H. Reiff, and W. J. Burke, "Response of Magnetotail Plasma at Lunar Distance to Changes in the Interplanetary Magnetic Field, the Solar Wind Plasma, and Substorm Activity," *Journal of Geophysical Research*, **84**, 1382, 1979.

Heikkila, W. J., "Comment on Electric Field Evidence on the Viscous Interaction at the Magnetopause, by F. S. Mozer," *Geophysical Research Letters*, **13**, 233, 1986.

Hill, T. W., "The Origin of the Plasma Sheet," *Reviews of Geophysics and Space Physics*, **12**, 379, 1974.

Howe, H. C., and J. H. Binsack, "Explorer 33 and 35 Plasma Observations of Magnetosheath Flow," *Journal of Geophysical Research*, **77**, 3334, 1972.

Iijima, T., and T. A. Potemara, "Field Aligned Currents in the Dayside Cusp Observed by TRIAD," *Journal of Geophysical Research*, **81**, 5971, 1976.

Lotko, W., B. U. O. Sonnerup, and R. L. Lysak, "Nonsteady Boundary Layer Flow Including Ionospheric Drag and Parallel Electric Fields," *Journal of Geophysical Research*, **92**, 8635, 1987.

McCoy, J. E., R. P. Lin, R. E. McGuire, L. M. Chase, and K. A. Anderson, "Magnetotail Electric Fields Observed From Lunar Orbit," *Journal of Geophysical Research*, **80**, 3217, 1975.

Mitchell, D. G., F. Kutchko, D. J. Williams, T. E. Eastman, L. A. Frank, and C. T. Russell, "An Extended Study of the Low-Latitude Boundary Layer on the Dawn and Dusk Flanks of the Magnetopause, "*Journal of Geophysical Research*, **92**, 7394, 1987.

Moses, J. J., N. U. Crooker, D. J. Gorney, and G. L. Siscoe, "High-Latitude Convection on Open and Closed Field Lines for Large IMF B_y," *Journal of Geophysical Research*, **90**, 11,078, 1985.

Mozer, F. S., "Electric Field Evidence on the Viscous Interaction at the Magnetopause," *Geophysical Research Letters*, **11**, 135, 1984.

Mozer, F. S., "Reply to Heikkila," *Geophysical Research Letters*, **13**, 235, 1986.

Olson, W. P., "A Model of the Distributed Magnetospheric Currents," *Journal of Geophysical Research*, **79**, 3731, 1974.

Olson, W. P., and K. A. Pfitzer, "Magnetospheric Boundaries and Fields," in *Correlated Interplanetary and Magnetospheric Observations*, edited by D. E. Page, p. 115, D. Reidel, Hingham, Mass., 1974.

Olson, W. P., and K. A. Pfitzer, "The Entry of AMPTE Lithium Ions Into a Magnetically Closed Magnetosphere," *Journal of Geophysical Research*, **89**, 7374, 1984.

Olson, W. P., and K. A. Pfitzer, "Magnetospheric Responses to the Gradient Drift Entry of Solar Wind Plasma," *Journal of Geophysical Research*, **90**, 10823, 1985.

Olson, W. P., K. A. Pfitzer, and S. L. Huston, "Final Report — Solar Wind Plasma in the Magnetosphere: Method of Entry and Consequences," MDC H3136, 1986.

Olson, C. L., and W. P. Olson, "Self-Consistent Gradient Drift Entry Model of the Magnetosphere Controlled by Limiting Currents," *EOS* Trans. AGU, **67**, 352, 1986.

Phan, T. D., B. U. O. Sonnerup, and W. Lotko, "Self-Consistent Model of the Low-Latitude Boundary Layer," *Journal of Geophysical Research*, **94**, 1281, 1989.

Reiff, P. H., and D. L. Reasoner, "The Magnetosheath Electron Population at Lunar Distance: General Features," *Journal of Geophysical Research*, **80**, 1232, 1975.

Rosenbauer, H., H. Grunwaldt, M. D. Montgomery, G. Paschmann, and N. Skopke, "Heos 2 Plasma Observations in the Distant Polar Magnetosphere: the Plasma Mantle," *Journal of Geophysical Research*, **80**, 2723, 1975.

Sanders, G. D., J. W. Freeman, and L. J. Maher, "A Two-Temperature Plasma Distribution in the Magnetosheath at Lunar Distances," *Journal of Geophysical Research*, **86**, 2475,1981.

Sarris, E. T., S. M. Krimigis, A. T. Y. Lui, K. L. Ackerson, L. A. Frank, and D. J. Williams, "Relationship Between Energetic Particles and Plasmas in the Distant Plasma Sheet," *Geophysical Research Letters*, **8**, 349, 1981.

Sonnerup. B. U. O., "Theory of the Low-Latitude Boundary Layer," *Journal of Geophysical Research*, **85**, 2017, 1980.

Spreiter, J. R., and S. S. Stahara, "A New Predictive Model for Determining Solar Wind-Terrestrial Planet Interactions," *Journal of Geophysical Research*, **85**, 6769, 1980.

Stevenson, T. E., and C. Comstock, "Particles Incident on Magnetic Field Gradients," *Journal of Geophysical Research*, **73**, 175, 1968.

Vestine, H. , "Some Comments on the Ionosphere and Geomagnetism," paper presented at XIVth General Assembly, Int. Union of Geomagn. and Aeron., Tokyo, Sept. 1963.

Wentworth, R. C., "Diamagnetic Ring Current Theory of the Neutral Sheet and Its Effects on the Topology of the Anti-Solar Magnetosphere," *Phys. Rev. Lett.*, 14, 1008, 1965.

Williams, D. J., and G. D. Mead, "Nightside Magnetosphere Configuration as Obtained From Trapped Electrons at 1100 Kilometers," *Journal of Geophysical Research*, 70, 3017, 1965.

Williams, D. J., D. G. Mitchell, T. E. Eastman, and L. A. Frank, "Energetic Particle observations in the Low-Latitude Boundary Layer," *Journal of Geophysical Research*, 90, 5097, 1985.

Williams, D. J., D. G. Mitchell, L. A. Frank, and T. E. Eastman, "Three-Dimensional Magnetosheath Plasma Ion Distributions," JHU-APL Preprint 87-28, submitted to JGR, 1987.

Zmuda, A. J., and J. A. Armstrong, "The Diurnal Variation of the Region With Vector Magnetic Changes Associated With Field Aligned Currents," *Journal of Geophysical Research*, 79, 2501, 1974.

Section 8

Publications and Presentations

Huston, S. L., K. A. Pfitzer, and W. P. Olson, Plasma Properties in the Magnetospher Determined From Gradient Drift Entry Model, MDSSC Report No. H5136-I, presented to 1989 Spring Meeting of the AGU, 7-12 May 1989.

The Impact of Magnetospheric Dynamic Processes on Hardware Systems in Low-Earth Orbit, presented to Air Force Geophysics Laboratory, Hanscom AFB, Mass., 12-14 September 1988.

Olson, W. P., The Contribution of Magnetospheric Currents to S_q, accepted for publication in *Journal of Applied Physics*.

Pfitzer, K. A., W. P. Olson, and T. S. Mogstad, A Time-Dependent, Source Driven Magnetospheric Magnetic Field Model, presented to the 1988 Spring Meeting of the AGU, May 16-20, 1988.

Olson, W. P., and K. A. Pfitzer, Response of Magnetotail Magnetic Field Topology to Changes in the North-South Component of the Interplanetary Magnetic Field, McDonnell Douglas Astronautics Company Report No. H2727-I, presented to the 1988 Spring Meeting of the AGU, May 16-20, 1988.

Huston, S. L., K. A. Pfitzer, T. S. Mogstad, and W. P. Olson, Predictions of Plasma Parameters in the Low-Latitude Boundary Layer and Plasma Sheet Using Gradient Drift Entry Theory, McDonnell Douglas Astronautics Co. Report No. H2645-I, presented to the 1987 Fall Meeting of the AGU, December 6-11, 1987.

Olson, W. P., and K. A. Pfitzer, Use of Geosynchronous Magnetometer Measurements to Estimate Solar Wind Parameters, McDonnell Douglas Astronautics Co. Report No. H2646-I, presented to the 1987 Fall Meeting of the AGU, December 6-11, 1987.

Olson, W. P., K. A. Pfitzer, and S. L. Huston, The Topology of the Parallel Currents Flowing Into and Out Of the Ionosphere, McDonnell Douglas Astronautics Co. Report No. H2593-I, presented at the IUGG XIX General Assembly, 10-22 August 1987.

Pfitzer, K. A., and W. P. Olson, The Entry of Magnetic Waves into the Magnetosphere and the Effect on the Plasma Sheet, McDonnell Douglas Astronautics Co. Report No. H2584-I, presented at the IUGG XIX General Assembly, 10-22 August 1987.

Huston, S. L., K. A. Pfitzer, and W. P. Olson, Variations of Plasma Velocity Distribution Functions Across the Low-Latitude Boundary Layer Driven by the Gradient Drift Entry Process, McDonnell Douglas Astronautics Co. Report No. H2585-I, presented at the IUGG XIX General Assembly, 10-22 August 1987.

Huston, S. L., K. A. Pfitzer, C. L. Olson, and W. P. Olson, Magnetospheric Response to Gradient Drift Entry of Solar Wind Plasma, McDonnell Douglas Astronautics Co. Report No. H2586, presented to the 1987 Spring Meeting of the AGU, 18-22 May 1987.

APPENDIX A

PARTICLE SPECTRA IN THE MAGNETOSHEATH

AND THE PLASMA SHEET

INTRODUCTION

Since the gradient drift entry process depends intimately on the particle energy spectrum in the magnetosheath, and since it determines the spectrum in the plasma sheet, a review of the general features of these spectra is in order. Many papers exist in the open literature discussing measurements made in these regions. However, many of these deal with measurements made in the dayside magnetosheath, and are thus of little interest since we are concerned mainly with the tail. Ideally, the data should include spectra from the magnetosheath and the plasma sheet in one pass, i.e., a traversal of the LLBL. We would also like to have simultaneous electron and proton data. Since our model of the GDE process is mainly valid for quiet conditions, it is also desirable that the spectra be taken during "quiet" magnetospheric intervals. Finally, we would like data from several locations in the magnetotail, covering the range from about X_{gsm}=-10 R_E out to lunar orbit.

Several papers have been found in the literature which present particle spectra from the magnetosheath and the plasma sheet. Most of these data were obtained from the IMP and ISEE spacecraft near the Earth (within about 20 R_E) and by instruments placed on the moon during the Apollo missions. This appendix discusses some of the general features of these spectra and how they relate to our study of the GDE process, with an emphasis on those spectra which are of most interest to this study, i.e., those which meet most of the criteria outlined above.

In analyzing these spectra, the spectra were first digitized from the papers, then a nonlinear least-squares curve fitting routine was used to fit distribution functions to the spectra. It was found that almost all of the spectra were fit well by kappa-distributions (*Formisano et al.* [1973], Chan *et al* [1975]) given by:

$$f_\kappa = \frac{\Gamma(\kappa+1)}{\pi^{3/2} \, \kappa^{3/2} \, \Gamma(\kappa-\frac{1}{2})} \, \frac{n}{V_T^3} \, (1 + \frac{|\Delta V|^2}{\kappa V_T^2})^{-(\kappa+1)}$$

where: f_κ = distribution function

V_T = characteristic thermal speed

$$= (\frac{2\kappa-3}{\kappa} \, \frac{kT}{m})^{1/2}$$

$|\Delta V|^2 = v^2 + V_s^2 - 2vV_s\cos\theta$

θ = angle between observed particle velocity v and bulk flow velocity V_s

Γ = gamma function

The spectra and fits are reproduced here; in order to facilitate comparison of the spectra, they are all plotted on similar scales.

PROTON SPECTRA

Three primary sources were found for proton spectra. Two of these present spectra from the plasma sheet and the magnetosheath during traversals of the LLBL. The third source does not present spectra from LLBL traversals, but the magnetosheath spectra are useful for comparison purposes. Table 1 shows the curve fit parameters for the magnetosheath and plasma sheet spectra, including the

Table 1. Curve fits to magnetosheath and plasma sheet proton spectra discussed in this appendix. Also given where available are the daily sum of K_p for each day and the daily average AE index as rough indicators of magnetospheric activity. See text for sources of spectra.

Spacecraft	Date	Daily Sum K_p	Daily Mean AE	Magnetosheath fits				Plasma sheet fits		
				κ	Number Density n (m^{-3})	Bulk Flow Speed V_s (m/sec)	kT (eV)	κ	Number Density n (m^{-3})	kT (eV)
ISEE-1	1/12/78	87	49	3	2.2×10^6	1.5×10^5	446	3	2.4×10^5	1440
ISEE-1	12/19/77	50	-	4	4.3×10^7	1.6×10^5	103	5	1.4×10^6	1290
(hot)				8	3.7×10^5	0	3055			
ISEE-1	7/7/78	217	-	4	2.2×10^7	2.4×10^5	228	4	7.6×10^5	4008
(hot)				6	3.3×10^5	0	4802			
HEOS 1	(composite)	-	-	2	4.3×10^7	2.5×10^5	696			
HEOS 2	12/13/72	327	461	4	5.9×10^6	3.9×10^5	181			
IMP 4	11/6/67	90	51	2	1.5×10^6	2.8×10^5	335			
IMP 5	11/7/69	213	208	7	9.1×10^6	1.3×10^5	247			

parameter kappa, number density n, bulk flow speed V_s, and temperature kT. Also shown are the daily sum of K_p for the days the spectra were taken and the daily average of AE (these were obtained from *NSSDC* [1987]). For two of the spectra a simple did not give an adequate fit to the data; in these cases a two-component distribution was obtained, consisting of a high-density "cold" component and a low-density "hot" component. For these spectra the "hot" component fit appears as a separate line below the "cold" component.

Chan et al. [1977] report proton spectra in the magnetosheath and plasma sheet from several sources. Magnetosheath spectra include:

o A composite spectrum measured by HEOS-1 and reported by *Formisano et al.* [1973]

o A spectrum measured by HEOS-2 on 13 December 1972 and reported by *Rosenbauer et al.* [1975]

o A spectrum measured by IMP-4 on 6 November 1967 and reported by *Frank* [1970]

o   A spectrum measured by IMP-5 on 7 November 1969 and reported by *Frank*
    [1971].

Plasma sheet spectra include:

o   Spectra measured by Vela-3B on 8 October 1965, 17 October 1965, and 8 April
    1966 and reported by *Hones et al.* [1971]

o   A spectrum measured by Vela-4B on 27 October 1967 and reported by *Hones et
    al.* [1972]

o   Spectra measured by OGO-3 on 14-15 June 1966 reported by *Frank* [1967].

Unfortunately, since these spectra were all taken at different times, they are of
little use for testing the GDE theory. They do, however, provide a reference with
which to compare other spectra. The spectra and fits are shown in Figure 1.

Eastman et al. [1985] present spectra for several passes through the LLBL by
the LEPEDEA instrument on the ISEE-1 spacecraft. One set of spectra is
particularly applicable, since it occurs in the dawn flank of the tail during a very quiet
interval. Spectra for the magnetosheath and the plasma sheet are given. Although
spectra are given for several other passes, this pass is of particular interest, and it
was the one used as the basis for the entry calculations performed in this study.
The magnetosheath and plasma sheet spectra are both shown in Figure 2.

Several features should be noted concerning these spectra. First, this is a very
quiet day, with the daily sum $K_p=87$, or an average of $K_p=1$. Second, the fluxes are
quite low compared to most of the other spectra discussed in this appendix. The
peak flux falls near the low range of the spectra listed in *Chan et al.*, and are about
two orders of magnitude lower than the spectra shown in *Williams et al.* [1987]. It
can also be seen that the high-energy tail of the plasma sheet spectrum merges
smoothly with that of the magnetosheath spectrum.

Williams et al. [1987] present spectra in the magnetosheath and plasma sheet for two intervals: on the dawn side on 19 December 1977 and on the dusk side on 7 July 1978. All spectra were taken using the LEPEDEA and MEPI instruments on the ISEE-1 spacecraft; the advantage of this is that the MEPI measurements extend the energy range up to over 100 keV, and some spectral characteristics can be discerned which would not be seen using the LEPEDEA data alone. For both of these intervals, several spectra are given for the magnetosheath. In Figures 3 and 4 these spectra are all plotted together. Although details of the spectra do differ somewhat, the general trends are similar, as can be seen in the figures. For each pass only one spectrum is given for the plasma sheet; these spectra are shown in Figures 5 and 6.

Two fairly striking features are apparent in the spectra for both intervals. First, both sets of magnetosheath spectra show two distinct populations, a low-energy, low-temperature population and a high-energy, high-temperature population. The low-energy populations have temperatures of 100-250 eV, and bulk flow speeds on the order of 150-250 km/sec. The high-energy populations have temperatures on the order of 3000-5000 eV, and the bulk flow speed appears to be approximately zero. In reality, these populations may have flow speeds nearly the same as the low-energy populations, but the bulk flow speeds would be small compared to the thermal speeds. A similar two-temperature population was reported in the magnetosheath at lunar orbit by *Sanders et al.* [1981].

The second striking feature in these spectra is that, as with the spectra reported by *Eastman et al.*, the plasma sheet spectra merge smoothly into the high-energy part of the magnetosheath spectra. In the case of *Eastman et al.*, however, no high-temperature component was observed; in this case, the plasma sheet spectrum appears to be similar to the high-temperature population observed in the sheath. For the spectra taken on the dawn side on 19 December 1977 (during quiet conditions), the density and temperature obtained for the plasma sheet differ considerably from those for the high-temperature component of the sheath. For the dusk side spectra obtained on 7 July 1978 (during moderately disturbed conditions),

on the other hand, the density and temperature obtained for the plasma sheet are quite close to those obtained for the sheath.

Williams et al. conclude that the low-energy portion of the spectrum is consistent with shocked solar wind plasma flowing along the flanks of the magnetosphere. For the dawn side traversal they conclude that the high-energy tail probably consists of plasma of magnetospheric origin; for the dusk side traversal they conclude that the high-energy tail is solar wind plasma which has been accelerated at the bow shock.

ELECTRON SPECTRA

Only one source was found which presented electron spectra in both the plasma sheet and the magnetosheath; this was Eastman et al. [1985]. Other sources give electron spectra in either the plasma sheet or the sheath, but not both. We present here spectra from Reiff and Reasoner [1975] which include both the dawn and dusk flanks of the magnetosheath at lunar orbit. Table 2 presents the curve fit parameters obtained for the magnetosheath electron spectra. For all these spectra, it was found that a single kappa-distribution did not provide an adequate fit to the measured spectra, and a two-component distribution was used. For both components the bulk flow velocity V_s was assumed to be zero; this is consistent with observations [Chan et al., 1977; Reiff and Reasoner, 1975] which indicate that the electron distribution is generally isotropic in the magnetosheath. Note, however, that this apparent isotropy may be due to the high thermal speed of the electrons, which typically is on the order of 10^6 m/sec, much higher than the ion bulk flow speed, which is typically on the order of 10^5 m/sec.

Eastman et al. [1985] present electron spectra in the magnetosheath and the plasma sheet taken during the same LLBL crossing as the proton spectra discussed previously. Thus these spectra provide an excellent test of the GDE theory. The

Table 2. Curve fits to magnetosheath electron spectra.

Spacecraft	Date	Daily Sum K_p	Daily Mean AE	Low-energy component			High-energy component		
				κ	Number Density n (m^{-3})	kT (eV)	κ	Number Density n (m^{-3})	kT (eV)
ISEE-1	1/12/78	87	49	5	4.7×10^5	69	6	1.0×10^4	423
CPLEE	4/6/71			10	5.1×10^6	17	5	5.8×10^4	106
CPLEE A	2/12/71			5	5.9×10^6	17	7	1.4×10^5	244
CPLEE B	2/12/71			5	5.9×10^6	17	7	4.6×10^4	205

magnetosheath spectrum shows a distinct two-temperature distribution, with a high-density, low-temperature component and a low-density, hot component. Unfortunately, the spectra do not extend to high enough energies to do a really good curve fit to the hot portion of the spectrum. The plasma sheet spectrum taken during the same interval has higher fluxes in the energy range 200-5000 eV. These spectra are shown in Figure 7.

Reiff and Reasoner [1975] present electron spectra through the magnetosheath during two passes of the moon through the dawn and dusk flanks of the sheath; these spectra are shown in Figures 8 and 9. Note that for the spectra taken during the dawn side traversal on 12 February 1971 the two detectors (A and B) measured two very different spectra in the high-energy tail. Detector A was oriented so that it looked more nearly into the magnetosheath bulk flow direction. Note also that these spectra are considerable denser and cooler than those reported by *Eastman et al.*; typical density of the low-energy component is 5×10^6 vs. 5×10^5, and typical temperatures are 17 eV vs. 69. Similar trends are seen in the high-energy components. The spectra taken by *Eastman et al.* appear to have been taken during a period of very low plasma density (the proton spectra were also among the least intense included in this survey).

DISCUSSION

The cases discussed above admittedly do not constitute a thorough statistical study. However, some general comments may be made concerning the plasma populations in the magnetosheath and the plasma sheet and how they relate to each other.

For protons in the magnetosheath, the bulk of the population is typical of shocked solar wind plasma. Number density ranges from approximately 0.3 to 50 cm^{-3}, bulk flow velocity ranges from about 100 to 500 m/sec, and temperature kT ranges from about 100 to 700 eV. Often superimposed on this "cold" component is a "hot", high-density component, which is sometimes similar to the plasma sheet spectrum, but not always. This "hot" component has densities several orders of magnitude lower than the main component, and temperatures on the order of several thousand eV. The thermal velocity of this component is high compared to the bulk velocity of the main component, and it is difficult to determine from curve fitting methods whether this component is flowing with the main component or not.

Protons in the plasma sheet typically have a bulk flow speed near zero, densities about one or two orders of magnitude lower than in the sheath, and temperatures on the order of 1000-5000 eV. In this small sample we have not seen evidence of multiple populations in the plasma sheet.

Electrons in the magnetosheath often seem to exhibit a dual population. Again, the lower-energy population is typical of shocked solar wind electrons; number densities are on the order of 0.5 to 5.0 cm^{-3}, and temperatures are in the tens of eV. The high-energy component is closer to Maxwellian than the low-energy component, with higher values of the index kappa. While this high-energy component seems similar to the plasma sheet spectra, *Reiff and Reasoner* argue that this component originates at the bow shock, since the density is comparable to or greater than that in the plasma sheet, and is largest closer to the bow shock.

REFERENCES

Chan, K. W., D. M. Sawyer, and J. I. Vette, "A Model of the Near-Earth Plasma Environment and Application to the ISEE-A and -B Orbit," NSSDC/WDC-A-R&S 77-01, Goddard Space Flight Center, 1977.

Eastman, T. E., L. A. Frank, and C. Y. Huang, "The Boundary Layers as the Primary Transport Regions of the Earth's Magnetotail," *Journal of Geophysical Research*, **90**, 9541, 1985.

Formisano, V., G. Moreno, F. Palmiotto, and P. C. Hedgecock, "Solar Wind Interaction with the Earth's Magnetic Field 1. Magnetosheath," *Journal of Geophysical Research*, **78**, 3714, 1973.

Hones, E. W., Jr., J. R. Asbridge, S. J. Bame, and S. Singer, "Energy Spectra and Angular Distributions of Particles in the Plasma Sheet and Their Comparison with Rocket Measurements over the Auroral Zone," *Journal of Geophysical Research*, **76**, 63, 1971.

Hones, E. W., Jr.., J. R. Asbridge, S. J. Bame, M. D. Montgomery, S. Singer, and S.-I. Akasofu, "Measurements of Magnetotail Plasma Flow Made with Vela 4B," *Journal of Geophysical Research*, **77**, 5503, 1972.

Mitchell, D. G., F. Kutchko, D. J. Williams, T. E. Eastman, L. A. Frank, and C. T. Russell, "An Extended Study of the Low-Latitude Boundary Layer on the Dawn and Dusk Flanks of the Magnetosphere," *Journal of Geophysical Research*, **92**, 7394, 1987.

NSSDC, "Selected Geomagnetic and Other Solar-Terrestrial Physics Data of NOAA and NASA," CD-ROM, United States Department of Commerce, National Oceanic and Atmospheric Administration, 1987.

Reiff, P. H., and D. L. Reasoner, "The Magnetosheath Electron Population at Lunar Distance: General Features," *Journal of Geophysical Research*, **80**, 1232, 1975.

Rosenbauer, H., H. Grunwaldt, M. D. Montgomery, G. Paschmann, and N. Sckopke, "Heos 2 Plasma Observations in the Distant Polar Magnetosphere: The Plasma Mantle," *Journal of Geophysical Research*, **80**, 2723, 1975.

Sanders, G. D., J. W. Freeman, and L. J. Maher, "A Two-Temperature Plasma Distribution in the Magnetosheath at Lunar Distances," *Journal of Geophysical Research*, **86**, 2475, 1981.
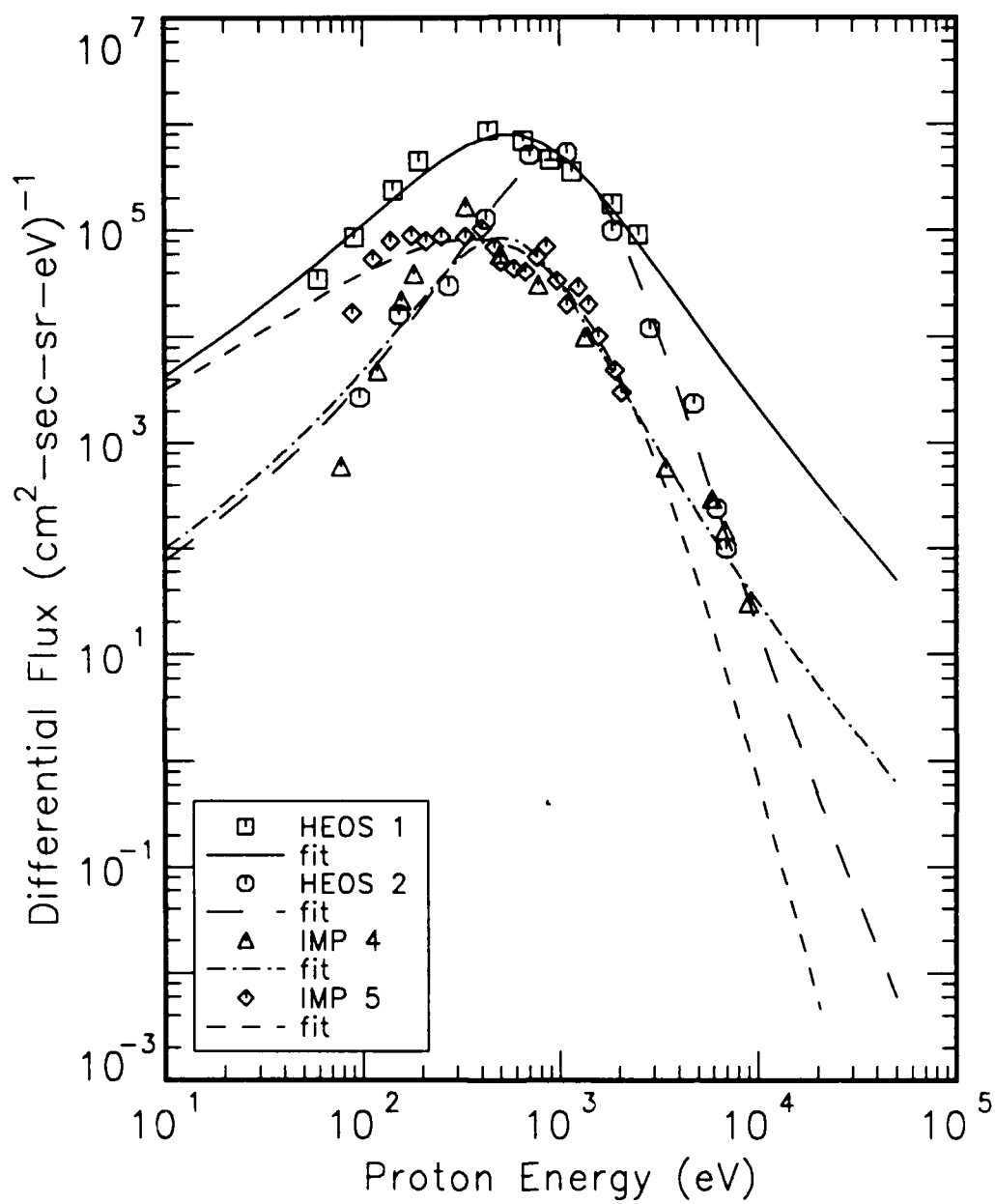
Figure 1.   Proton spectra in the magnetosheath compiled by *Chan et al.* [1977]. See text for sources of data.
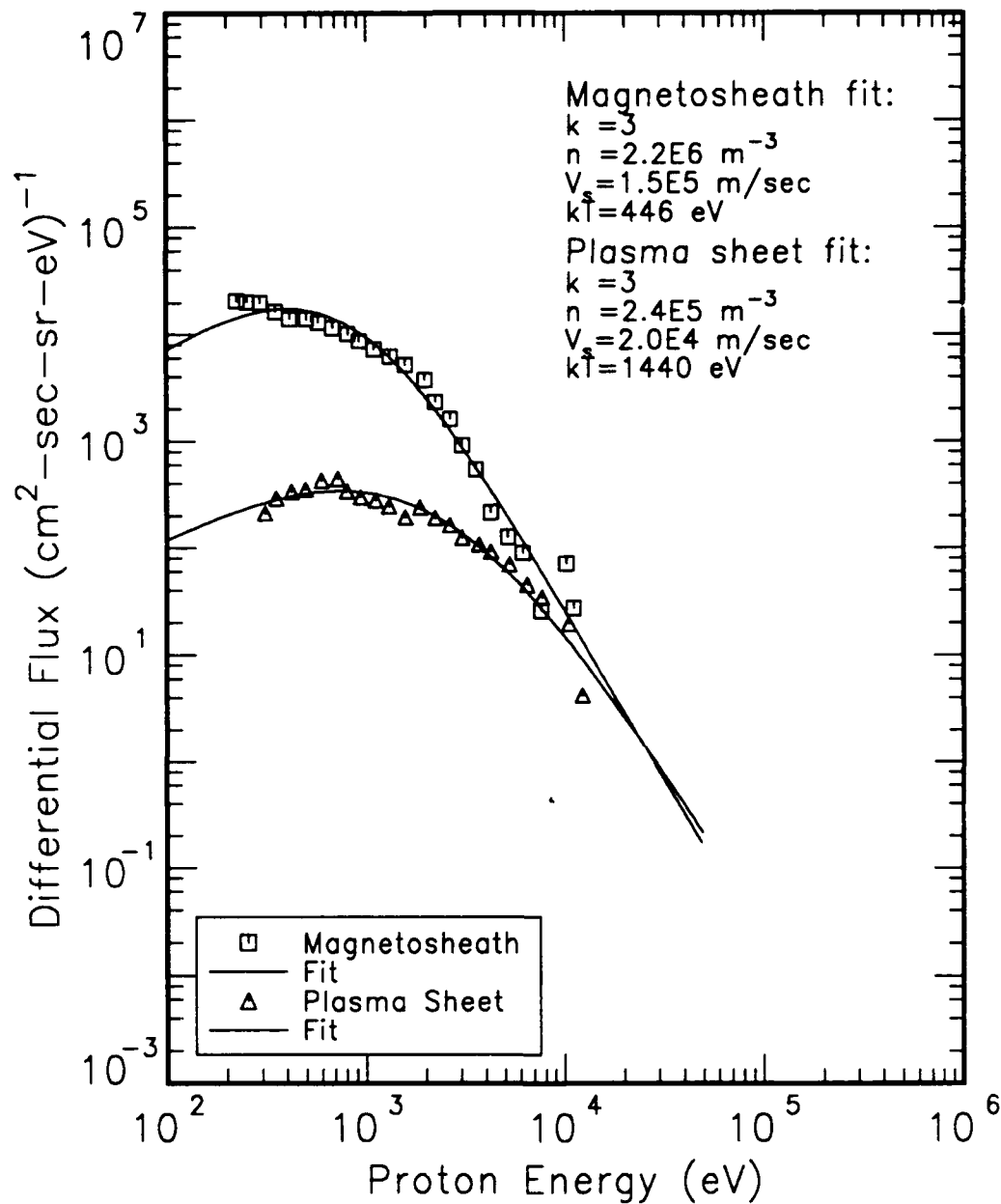
Figure 2. Proton spectra in the dawn magnetosheath reported by *Eastman et al.* [1985]. These spectra were taken during a single pass of the ISEE-1 spacecraft through the LLBL on 12 January 1978. Spectra were taken approximately five hours apart.
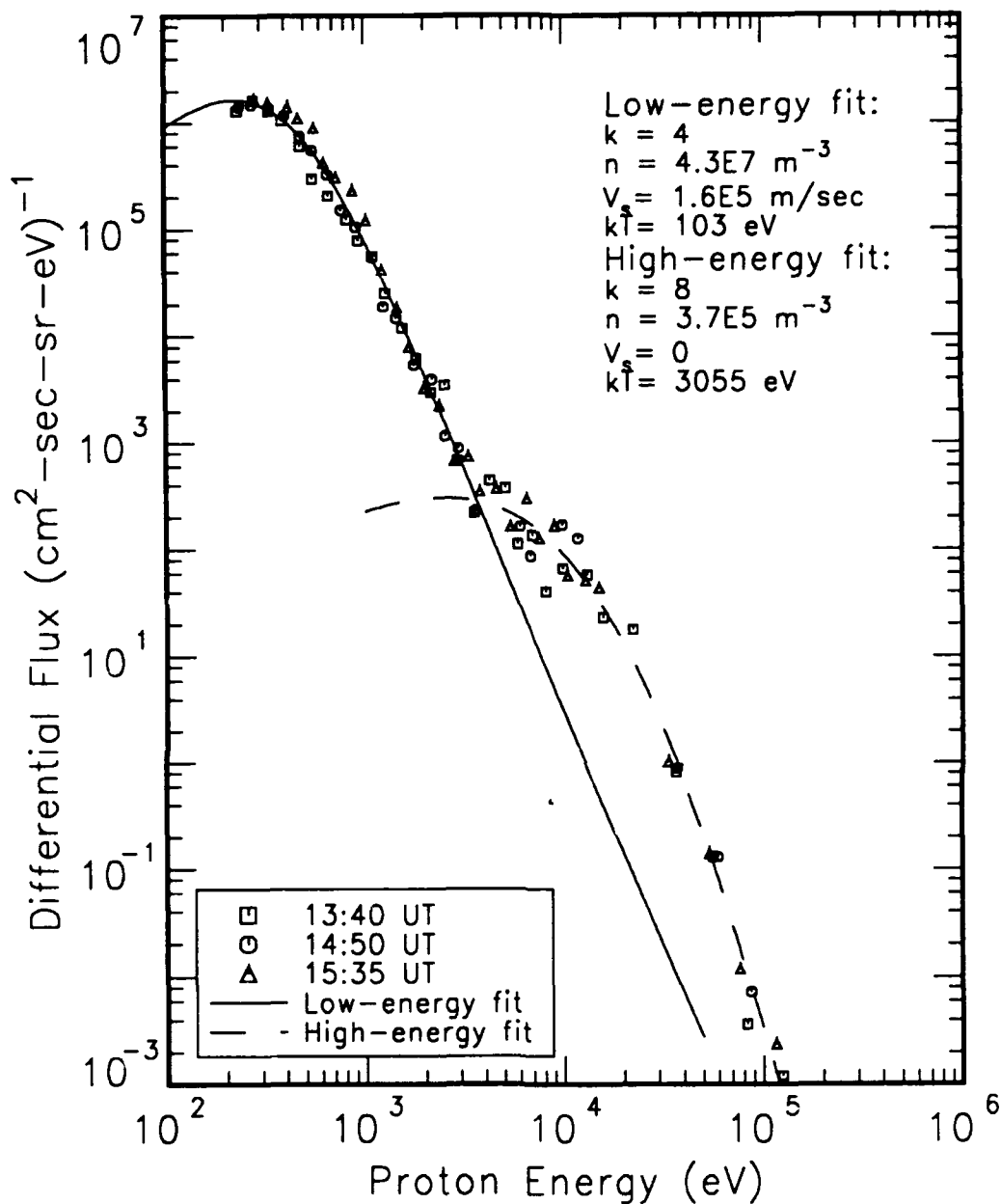
Figure 3.   Proton spectra taken in the dawn magnetosheath reported by Williams et al. [1987]. Spectra were taken with ISEE-1 LEPEDEA and MEPI instruments on 19 December 1977; universal times are given in the legend. A two-component kappa distribution fit is shown.
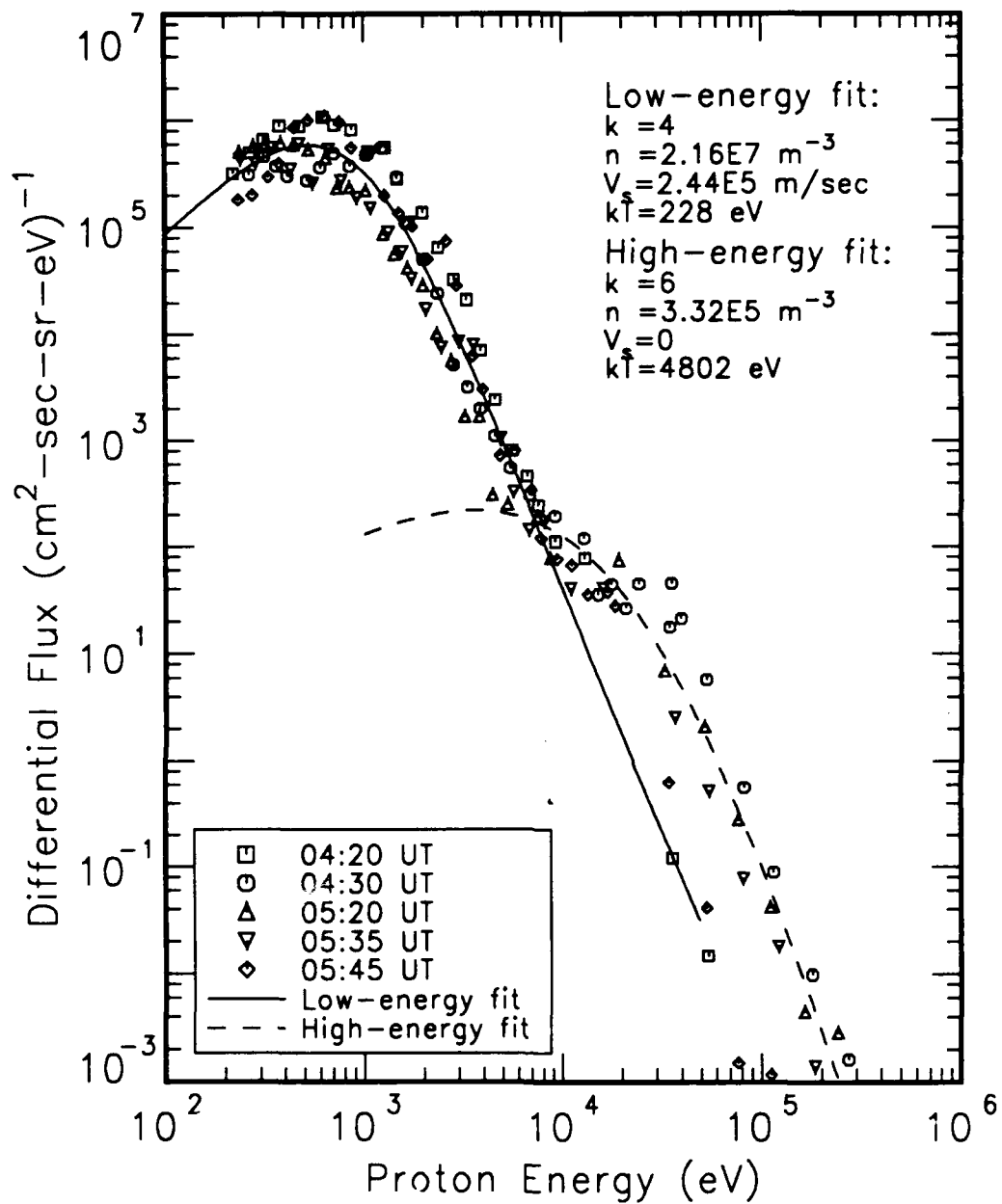
Figure 4.   Proton spectra taken in the dusk magnetosheath reported by Williams et al. [1987]. Spectra were taken with ISEE-1 LEPEDEA and MEPI instruments on 7 July 1978; universal times are given in the legend. A two-component kappa distribution fit is shown.
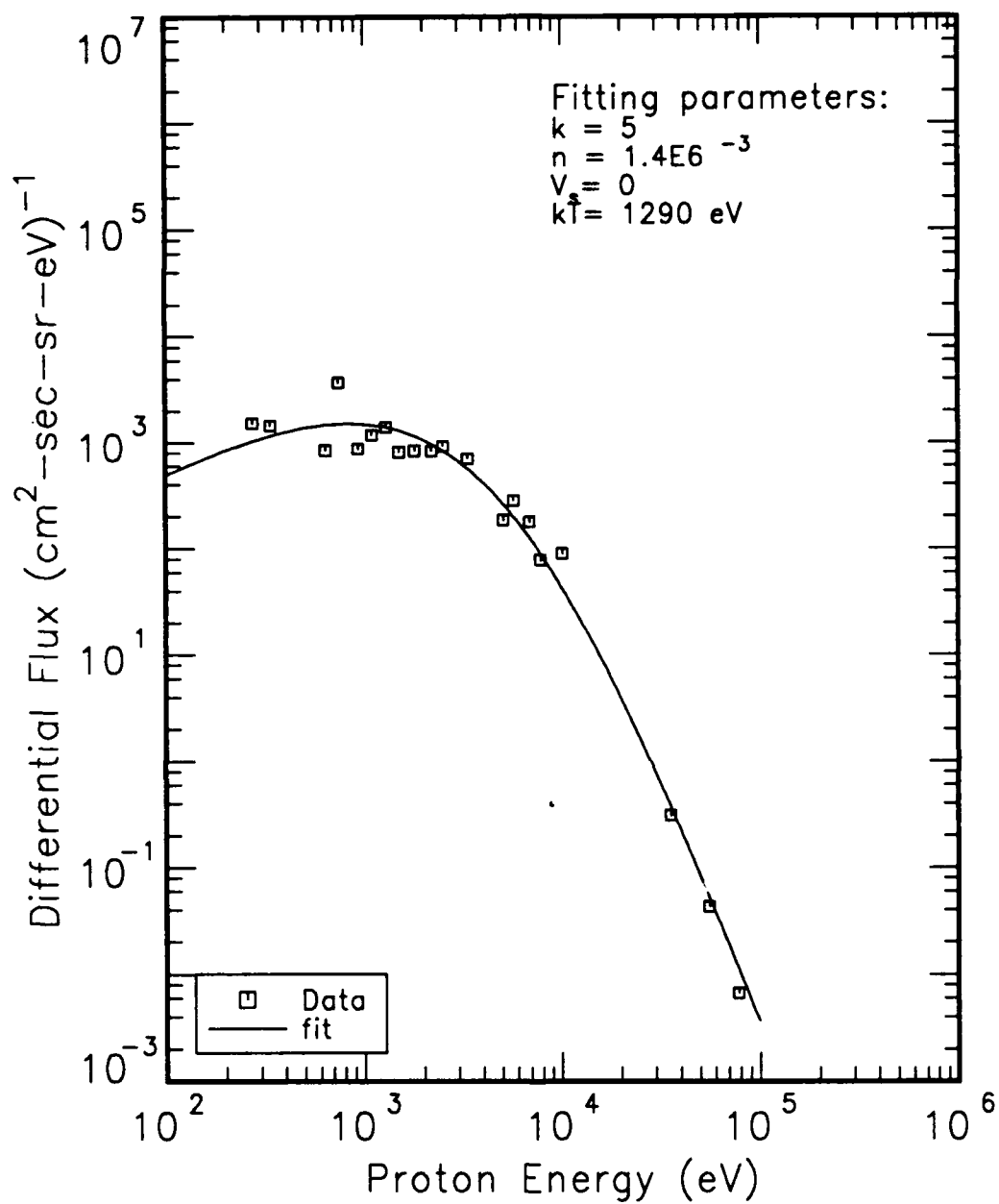
A-13

Figure 5.   Proton spectra in the plasma sheet reported by *Williams et al.* [1987]. Spectrum was taken at approximately 10:00 UT on 19 December 1977 during the same traversal of the LLBL as the spectra in Figure 3.
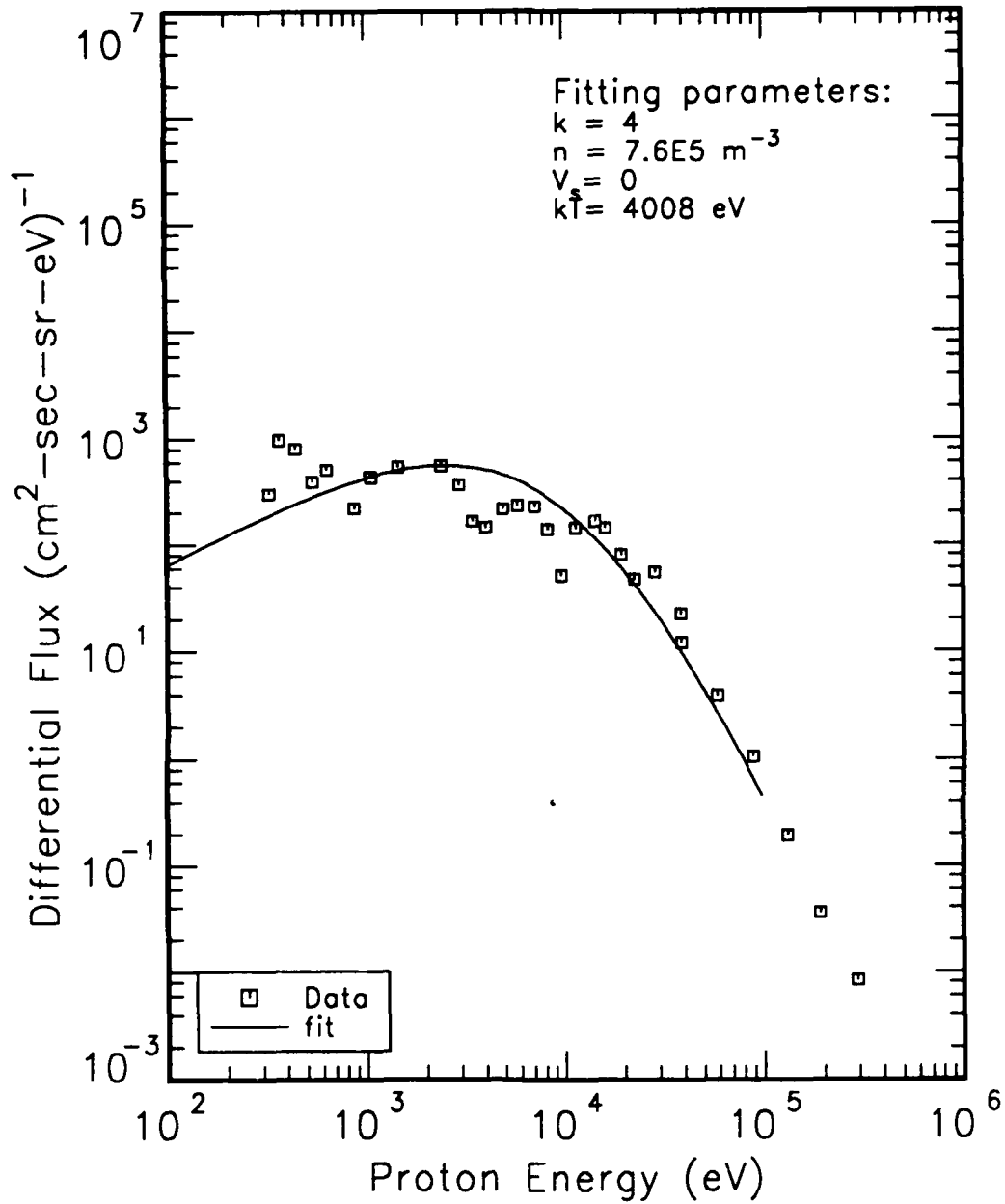
Figure 6.   Proton spectrum taken in the dusk side plasma sheet reported by *Williams et al.*
[1987]. Spectrum was taken at approximately 04:20 UT on 7 July 1978 during
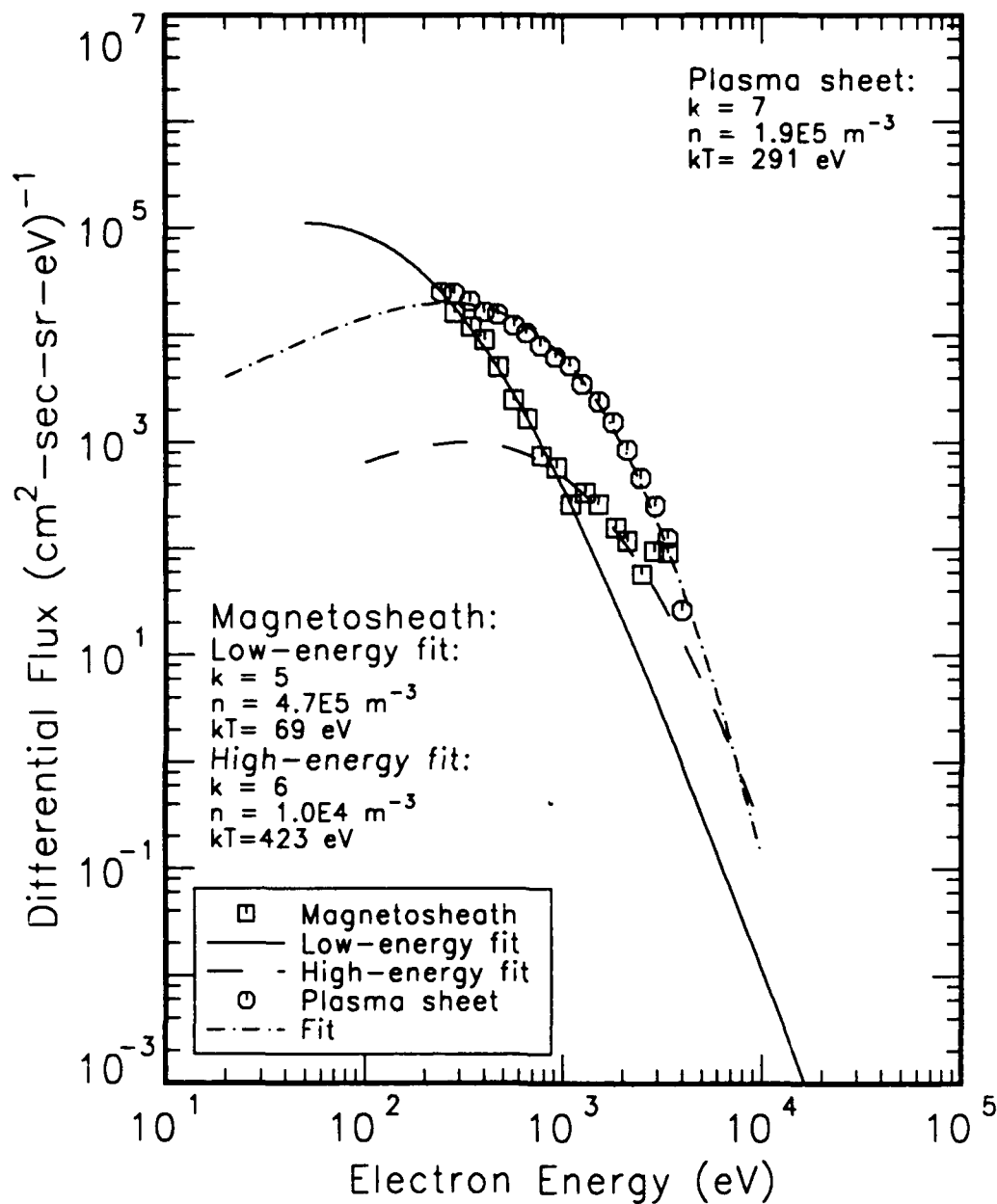the same traversal of the LLBL as the spectra in Figure 4.

Figure 7.   Electron spectra in the dawn magnetosheath and plasma sheet reported by
Eastman et al. [1985]. Spectra were taken during the same LLBL traversal as
the proton spectra shown in Figure 2.

10^7

10^5

10^3

10^1

10^{-1}

10^{-3}

Differential Flux $(cm^2-sec-sr-eV)^{-1}$

Low−energy fit
(Detectors A & B):
k =5
n =5.9E6 m^{-3}
kT=17 eV

Detector A:
k =7
n =1.4E5 m^{-3}
kT=244 eV

Detector B:
k =7
n =4.6E4 m^{-3}
kT=205 eV

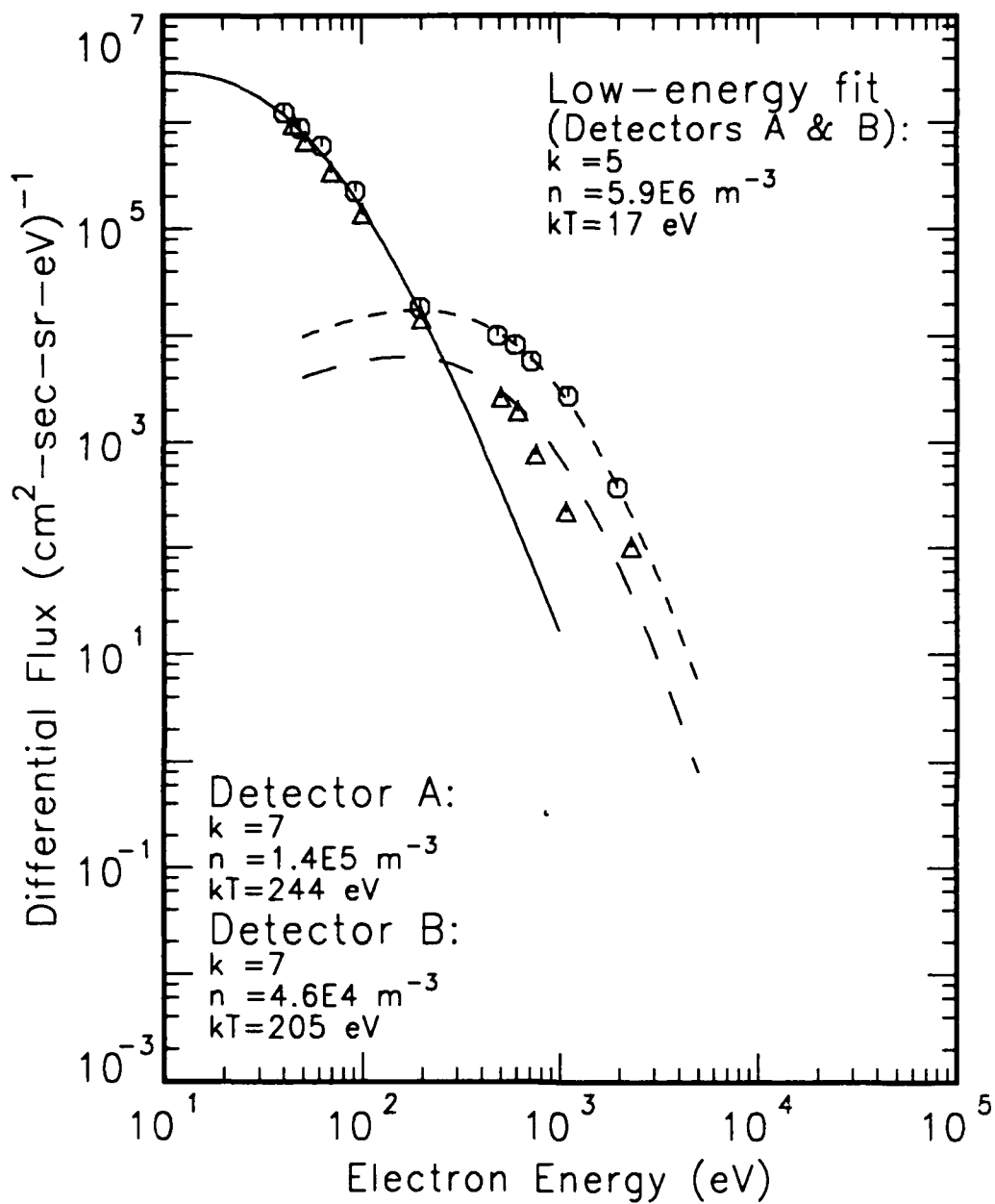10^1 10^2 10^3 10^4 10^5

Electron Energy (eV)

Figure 8.   Electron spectra in the dawn magnetosheath at lunar orbit reported by *Reiff and Reasoner* [1975].   Detector A (circles) faced approximately into the magnetosheath flow in the dawnside magnetosheath, and detector B (triangles) faced approximately 60 degrees west. The low-energy fit to data from both detectors is shown; individual high-energy fits are shown for each detector.
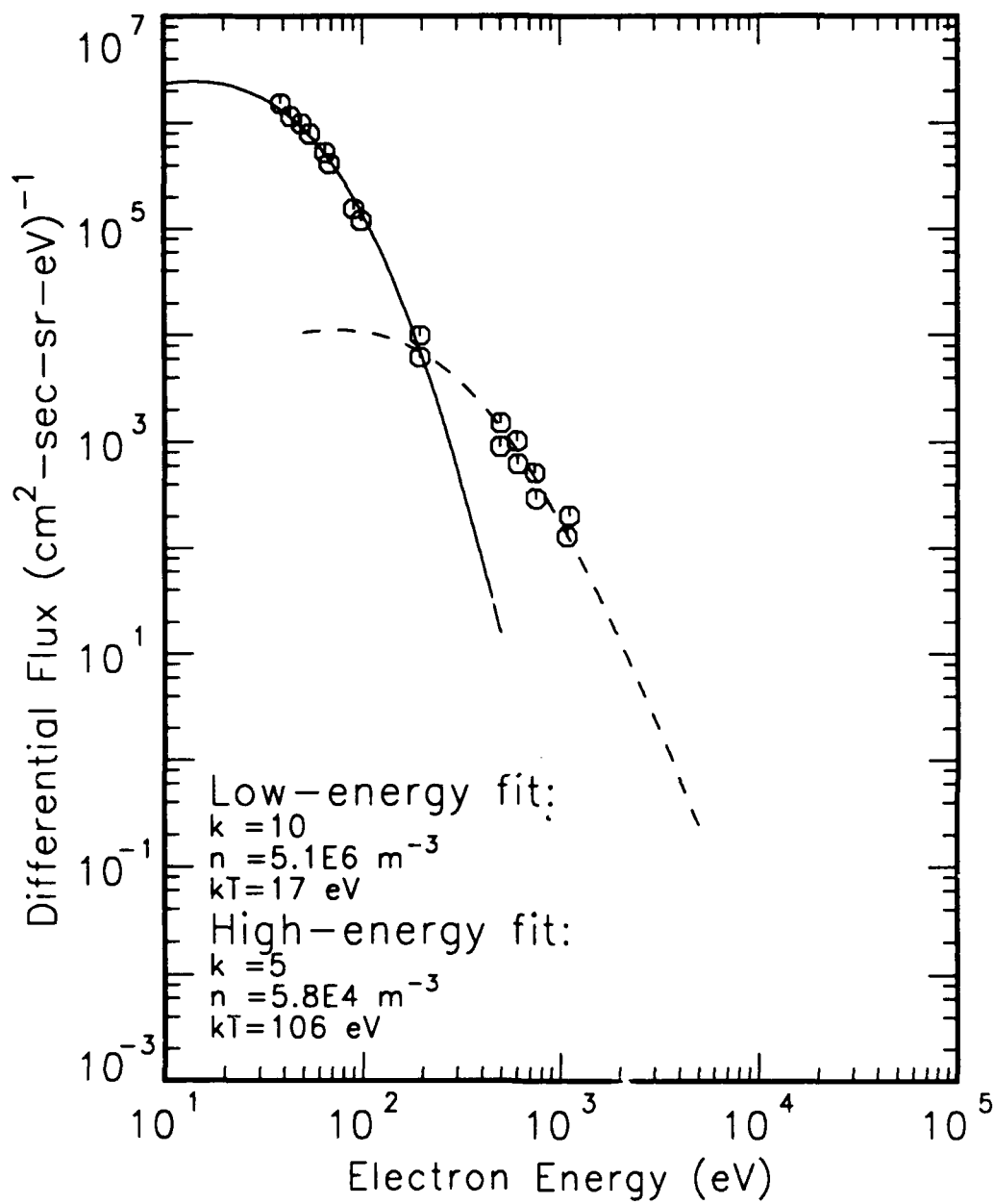
Figure 9.   Electron spectra in the dusk magnetosheath at lunar orbit reported by *Reiff and Reasoner* [1975]. The curve fits shown are to combined data from both CPLEE detectors.

Appendix B

Gas Dynamic Equations for Magnetosheath Flow

The flow of plasma within the magnetosheath has been modeled by applying the well-known gas dynamic equations for an ideal gas. In order to specify the flow conditions at the magnetopause, it is necessary to know the solar wind Mach number M_∞, the ratio of specific heats γ, and the local pressure p. By combining the normal shock and isentropic flow equations, the local density, velocity, and temperature can be determined for any point on the magnetopause.

The average value of the solar wind Mach number is about 8-10, with the vast majority of measurements between 6 and 12; for this study we have chosen a value of $M_\infty=10$. Typically, the ratio of specific heats γ is taken to be 5/3.

The major problem in determining the local properties along the magnetopause is determining the local pressure. If the shape of the magnetopause is known, the Newtonian approximation provides a reasonable value for the local pressure:

$$\frac{p}{p_\infty} = 1 + \gamma\, M_\infty{}^2 K \cos^2\theta_{mp} \tag{8}$$

where θ_{mp} is the local slope of the magnetopause given by

$$\theta_{mp} = \frac{\pi}{2} - \tan^{-1}\left(\frac{-dy_{mp}}{dx}\right) \tag{9}$$

and K is given by

$$K = \left(\frac{\gamma+1}{2}\right)^{(\gamma+1)/(\gamma-1)} \left[\gamma\,(\gamma - \frac{\gamma-1}{2\,M_\infty^2})^{1/(\gamma-1)}\right]^{-1} - \frac{1}{\gamma\,M_\infty^2} \tag{10}$$

With the local pressure computed, the remaining flow properties can be determined (here they are normalized by the corresponding solar wind properties).

Stagnation pressure p_s:

$$\frac{p_s}{p_\infty} = \frac{(\gamma + 1)\, M_\infty^2}{2} \left[\frac{(\gamma + 1)^2\, M_\infty^2}{2\,(2\,\gamma\, M_\infty^2 - \gamma + 1)} \right]^{1/(\gamma - 1)} \tag{11}$$

Mach number M:

$$M^2 = \frac{2}{(\gamma - 1)} \left[\left(\frac{p_s}{p_\infty}\, \frac{p_\infty}{p} \right)^{(\gamma - 1)/\gamma} - 1 \right] \tag{12}$$

Density ρ:

$$\frac{\rho}{\rho_\infty} = \frac{(\gamma + 1)\, M_\infty^2}{2 + (\gamma - 1)\, M_\infty^2} \left[\frac{(1 + \gamma)}{2\,\gamma\, M_\infty^2 - \gamma + 1}\, \frac{p}{p_\infty} \right]^{1/\gamma} \tag{13}$$

Velocity V:

$$\left(\frac{v}{v_\infty} \right)^2 = \left(\frac{M}{M_\infty} \right)^2 \frac{\rho_\infty}{\rho}\, \frac{p}{p_\infty} \tag{14}$$

$$= \frac{2}{(\gamma - 1)\, M_\infty^2}\, \frac{\rho_\infty}{\rho}\, \frac{p}{p_\infty} \left[\left(\frac{p_s}{p_\infty}\, \frac{p_\infty}{p} \right)^{(\gamma - 1)/\gamma} - 1 \right]$$

Temperature T:

$$\frac{T}{T_\infty} = \frac{2 + (\gamma - 1)\, M_\infty^2}{2 + (\gamma - 1)\, M^2} \tag{15}$$